Desalination and Water Treatment
www.deswater.com

doi: 10.5004/dwt.2021.27918

244 (2021) 302–324
December

Cellulose acetate based hybrids: fascinating material as a potential adsorbent for Congo red removal

Irum Asif[a,*], Uzaira Rafique[b]

[a]*Department of Environmental Sciences, Applied Chemistry Lab, Fatima Jinnah Women University, The Mall, Rawalpindi 46000, Pakistan, Tel. 0092 51 9292900 Ext. 2088; Fax: 0092 51 9292903; email: irumasif@fjwu.edu.pk (I. Asif)*
[b]*Applied Chemistry Lab, Fatima Jinnah Women University, The Mall, Rawalpindi 46000, Pakistan, Tel. +92 51 9292900 Ext. 1105; Fax: +92 51 9292903; email: uzairaiqbal@yahoo.com*

Received 14 May 2021; Accepted 23 October 2021

ABSTRACT

The present paper describes the synthesis of cellulose acetate based hybrid materials in the form of eco-friendly beads and fibres and state its performance feasibility in the uptake of industrially important dye (Congo red) from aqueous media at bench scale. Cellulose acetate (CA) based hybrid materials have attracted attention due to diverse applications as absorbent, purification, chemical separations etc. These materials have an added advantage that they can easily be moulded into membranes, fibres and beads cellulose acetate is selected due to their low cost, easy availability, non-toxicity, and natural biodegradability. A facile, novel and greener approach was applied for the incorporation of Al^{3+}, Ti^{4+}, $Zr^{4+,}$ and Si^{4+} moieties to form chemically and thermally stable CA based hybrids. The newly developed materials were characterized by proton NMR, XRD, FT-IR, TGA / DTA, EDX-SEM, and BET analysis. The SEM and BET results showed that synthesized hybrids have high pore volume and diameter with increased surface area as compared to the raw cellulose acetate. In this work, the removal efficiency of adsorbents was investigated as a function of varying dye concentration, temperature and solution pH. The batch adsorption experiments showed higher adsorptive capacities of hybrids over a pH range of 1–7 in comparison to base material. The results are in accordance with the pzc values, suggesting wider application of synthesized hybrids under different environmental conditions. The adsorption mechanism follows Ho's pseudo-second-order, and the equilibrium data fitted well with Langmuir model. Kinetic studies reveal physisorption phenomenon in synthesized hybrids following cooperative adsorption, as compared to normal adsorption in raw CA. The successful synthesis and application of CA based hybrids shows strong potential for the commercially viable, economical and alternate materials for efficient removal of different dyes from industrial effluents.

Keywords: Cellulose acetate; Hybrids; Beads; Fibres; Congo red; Adsorption kinetics; Models

1. Introduction

The removal of pollutants from wastewaters has been a subject of widespread industrial research. However, most of the processes applied today are unacceptable, owing to the disposal of sludge, their high price, low proficiency and limited applicability to few pollutants [1].

Adsorption is a well-known separation technique that recently emerged as one of efficient and economic methods for water decontamination applications [2]. Another advantage is that the adsorbents can be regenerated by suitable desorption processes due to the reversible nature of most adsorption processes. They can be applied multiple times by processes that are of low maintenance cost, high efficiency, and easy to operate [3].

* Corresponding author.

A number of adsorbents such as activated carbon, zeolites, clays and agricultural residues have been used [4] in the past but have drawbacks of low adsorption capacity, limited regeneration capability. Now the major challenge in this field is to synthesize novel materials with all the desired and controlled properties of a good adsorbents such as renewable, low-cost, and degradability [5]. The interest in the polymer science from the renewable resources increased significantly in recent years [6–10]. In these materials, the functional variation of organic materials is combined with advantages of a thermally stable and robust inorganic substrate, resulting in strong binding affinities toward selected metal ions and organic pollutants [11,12]. Recently, functionalized polymeric hybrids are regarded as one of the most effective adsorbents [13]. These kinds of materials often present the best properties of each of its components in a synergic way and have high performances of physical, chemical and mechanical properties [11].

Cellulose is the most abundant biopolymer that attracted a lot of attention due to its unique properties [14]. It is stated as "a fascinating and almost inexhaustible sustainable natural polymer" by Kargarzadeh et al. [15] The typical derivatives are carboxymethylcellulose (CMC), cellulose acetate (CA), methyl cellulose (MC), hydroxyethyl cellulose (HEC), (hydroxypropyl)methylcellulose (HPMC), and so on. Among all the derivatives, cellulose acetate (CA) has been extensively applied due to its solubility in organic and inorganic solvents [16].

Cellulose acetate (CA) is a very versatile biocompatible polymer and several strategies have been employed in an attempt to broaden its application including simple blending with other polymers, chemical modifications either by adding more functionalities or by grafting polymer chains on some other organic or inorganic precursors in the form of metal alkoxides [17]. Addition of metal oxides is reportedly applied to enhance the adsorbent properties of the polymer material either by covalent bonding or by physical interactions [18,19].

The reason for mixing compounds of different chemical nature is the synergy that can be obtained from species with dissimilar properties (e.g., polymer and metal oxide) in only one material. The synthesis of hybrid materials can be obtained through different ways, for example: melt intercalation, solution intercalation, and *in-situ* polymerization [20]. Recently, cellulose acetate based hybrid materials are prepared by the fabrication via water vapour induced phase inversion and simultaneous hydrolysis/condensation at ambient conditions [21]. In this work, a versatile synthetic route to functionalize oxygen bridged polymers will be used for the first time to prepare oxygen based hybrid materials with improved properties, which can be tailored as fibres/beads with potential industrial application as adsorbents. This unprecedented functionalization may open up new goals to obtain, owing to multiple environmental applications of polymer hybrids

2. Materials and methods

All reagents were of analytical grade and employed in experiments without prior purification: cellulose acetate polymer (M.W. 30,000) (95%) was obtained from UniChem Origin. Anhydrous glacial acetic acid (>99%), aluminium isopropoxide (>99%), zirconium chloride (>99%), ammonia solution (30%) and acetone (>99.5%) were obtained from Merck. Acetone was sieved through molecular sieves (Type-4 Å) to remove moisture and stored in dry condition prior to use. Triflouroacetic acid (99%) (tetraethoxy silane (>99%) and 3-aminopropyl trimethyl silicate (APTMS) (97%) were obtained from Scharlau. Titanium butoxide (>99%) was obtained from Dae-Jung, Korea.

2.1. Preparation of CA based hybrids

CA based hybrid materials were synthesized by adopting [22] the use of starting materials for mixing, that is, CA and aluminium (Fig. 1). Cellulose acetate (0.36 mmol, 0.1 g) was immersed in a solution containing a mixture (1:1 V/V) of acetone and glacial acetic acid till a homogeneous slurry was obtained. Appropriate amount (0.073 g; 0.36 mmol) of aluminium isopropoxide was dissolved in triflouroacetic acid in a separate container and mixed with solution A. The solution was stirred for 2 h. The mixture was slowly dropped in distilled water (pH 10.0) with constant stirring till fibres are formed. The material was filtered and washed with distilled water till the neutral pH is achieved. This procedure was applied for the first time for the synthesis of other CA based hybrid materials (CA-Si, CA-Ti and CA-Zr) by using equimolar ratios of TEOS/APTMS, titanium butixide (0.124 ml) and zirconium chloride (0.083 g) in place of aluminium isopropoxide.

2.2. Characterization

The following section details the techniques used for the hybrid characterisation. The salt addition technique [23,24] was performed to determine pzc value of the newly synthesized CA based hybrids. pzc provides important information about the adsorption mechanism. 0.2 g of the material was dispersed into 40.0 mL of 0.1 M $NaNO_3$ solution, whose pH (pHi) was adjusted to 2, 4, 6, 8, 10, and 12 (±0.1 pH units) with 0.1 M HNO_3 and 0.1 M NaOH. The samples were shaken for 24 h using a rotary agitator (SK-300 Lab Companion) at 200 rpm. After the end of agitation, the final pH was measured and plotted vs. the initial pH. The thermal stability of the hybrid materials (CA, CA-Al, CA-Si, CA-Ti and CA-Zr) was examined using a TGA 209 F3 thermogravimetric analyser (NETZSCH, Germany). Typically, the instrument was operated using nitrogen as the purge gas and a nominal flow-rate of 15 mL/min. Samples (~10 mg) were added to aluminium crucibles with lids and loaded into the TGA, a temperature profile where the samples were ramped from ambient to a final temperature of 800°C at a rate of 10°C/min. Mass loss as a function of temperature was recorded and the derivative traces were collected. For hybrid materials, TGA is an excellent method for determining the metal oxide content and its comparison with the parent polymer.

Infrared spectra were collected using a model 8400 Shimadzu (Japan) spectrophotometer, using KBr pellet conventional method. A resolution of 2 cm^{-1} was used, with spectra being averaged from 15 scans and a spectral window ranging between 4,000 and 400 cm^{-1}.

SEM-EDS was used to aid in the study of incorporation of the metal oxides in the polymer based hybrids. Morphological characterization is performed by (MAIA3 TESCAN) scanning electron microscope with an accelerating voltage of 20.0 kV. Prior to sample analysis, the hybrid materials were coated with a thin layer of gold alloy to minimize charging effects under electron beam irradiation. To measure the size of each particle, image J software was used and their size range and average size was measured. The measurement of XRD was carried out by XRD diffractometer (OPTICS-V5) Step size 0.02, Cu-K alpha radiations and angle of 0–180. Brunauer–Emmett–Teller (Micrometrix Tristar 3000) was used to measure the textural parameters like surface area and pore size distribution (pore volume and pore diameter) through multi-point adsorption-desorption method with Barrett–Joyner–Halenda (BJH) isotherm model. For this purposes, all the synthesized CA based hybrid materials were degassed at 423 K for 2 h on a vacuum line.

2.3. Adsorption batch experiments

The adsorption studies were carried out by using the orbital shaker are 100 rpm (model SK-300, Lab Companion, UK) and Congo red concentration was determined by using UV-Visible spectrophotometer (UV-1601) Shimadzu, Japan.

3. Results and discussion

3.1. ^{1}H NMR spectroscopic analysis

The ^{1}H NMR of CA based hybrids were recorded in DMSO is shown in Table 1. All chemical shifts (δ) were given in parts per million downfield from tetramethyl silane (TMS) as internal standard. The peaks at 1.872–2.503 ppm corresponds to the three methyl group protons of acetyl groups and peaks at 3.366–5.691 ppm represent the seven anhydrglucose protons [25–28] confirming the presence of cellulose acetate in the synthesized hybrids. Since, the technique was not able to confirm the presence of inorganic moieties, other techniques were applied to further characterize the synthesized hybrids.

3.2. X-ray diffraction method

The X-ray diffractrograms of CA based hybrids are depicted in Fig. 2. The material presents a structure mostly amorphous, once no crystalline peak was observed [29]. CA and the synthesized hybrids do not show sharp peaks, mainly due to the reason that they possess low degree of crystallinity [29,30]. The less degree of crystallinity is due to the substitution of the hydroxyl groups by acetyl groups with greater volume, which broke the inter- and intramolecular hydrogen bonds of cellulose [31,32]. Broad band around 15° and 30° can be attributed to inorganic fraction characterized by amorphous silica material confirming the presence of cellulose acetate in the hybrids [33,34].

3.3. Fourier-transform infrared spectroscopic analysis

FTIR spectra of the synthesized hybrids are presented in Fig. 3 and compared with the spectrum of pure amorphous cellulose acetate fibres. The major characteristic absorption bands for cellulose acetate are assigned as follows: 3,800–3,300 cm^{-1} (–OH), the methylene asymmetric stretching at 2,965–2,850 cm^{-1} (–CH_2), carbonyl stretching at 1,740 cm^{-1} (–C O O of –COOR), CH_2 bending or OH in plane bending at 1,444 cm^{-1}, alkoxyl stretch of the ester at 1,255 cm^{-1} (C–O–C), methyl bending at 1,372.7 cm^{-1} (C–CH_3), C–O–C antisymmetric bridge stretching at 1,167 cm^{-1}, acetyl linkage at 1,039.8 cm^{-1}, as reported in literature [34–36].

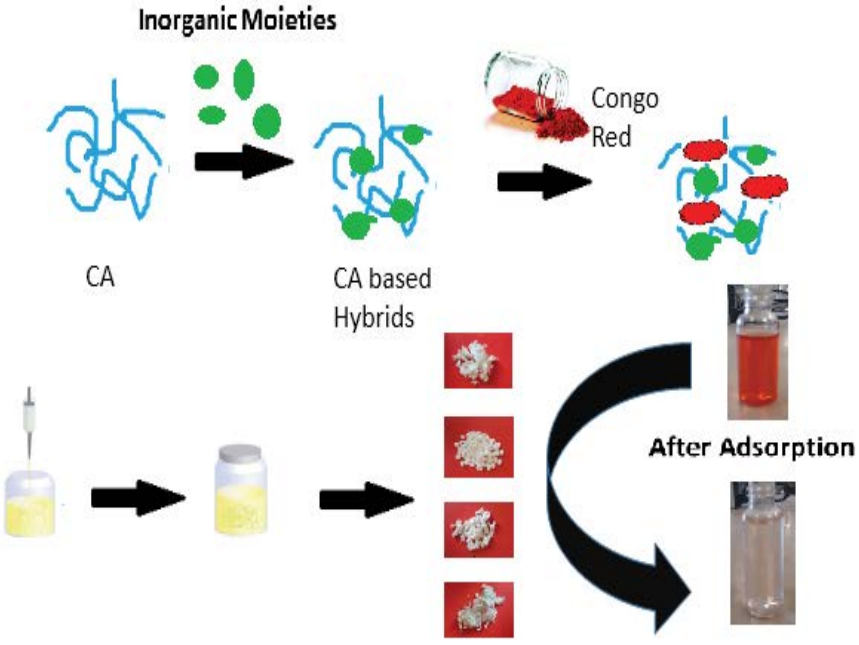

Fig. 1. Schematic presentation of the synthesis of hybrids and its application in Congo red removal.

The FTIR spectrum of the CA based hybrids CA-Al, CA-Si, CA-Ti and CA-Zr show similar characteristic bands as mentioned above, indicating that cellulose acetate matrix is not affected in the hybrids. The signal at around 1,091 cm^{-1} representing Al–O bond confirms the presence of Al^{3+} in the CA-Al hybrids [37]. In the FTIR spectrum of the CA-Si, the weak peak at 1,067 cm^{-1} is assigned to the asymmetric Si–O stretching mode [22]. The formation of Si–O–Si groups might be ascribed to self-hydrolysis/condensation of APTMS and TEOS during the phase inversion process. [38]. It suggested the formation of the chemical bonds between SiO_2 by condensation reaction between TEOS and APTMS. Whereas, in FTIR spectrum of CA-Ti, the weak peak at 785 cm^{-1} corresponded to Ti–O–Ti stretching modes, as reported in earlier findings [39,40]. At the lower region of spectrum, the band at 500 cm^{-1} is due to Ti–O bond bending vibrations [41]. In the FTIR spectrum of CA-Zr, an additional peak at 528 cm^{-1} is due to the superposition of metal–oxygen stretching vibrations confirming binding between Zr–O–Zr [42,43].

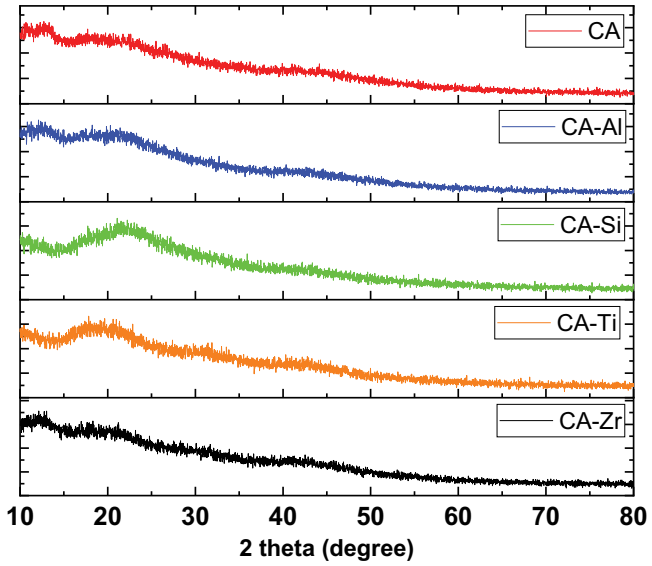

Fig. 2. XRD spectrum of cellulose acetate based hybrids (CA, CA-Al, CA-Si, CA-Ti and CA-Zr).

3.4. Thermogravimetric analysis

The incorporation of various types of metals into the cellulose acetate matrix is one of the new breakthroughs in improving their adsorption efficiency in different environmental conditions. TGA was used to study the thermal analysis of CA based hybrid materials as shown in Fig. 4. As observed from the thermograms, from room temperature till 100°C, the TGA curves display a slight mass loss attributed to the moisture due to water desorption, indicating hydrophobic nature of the products. The

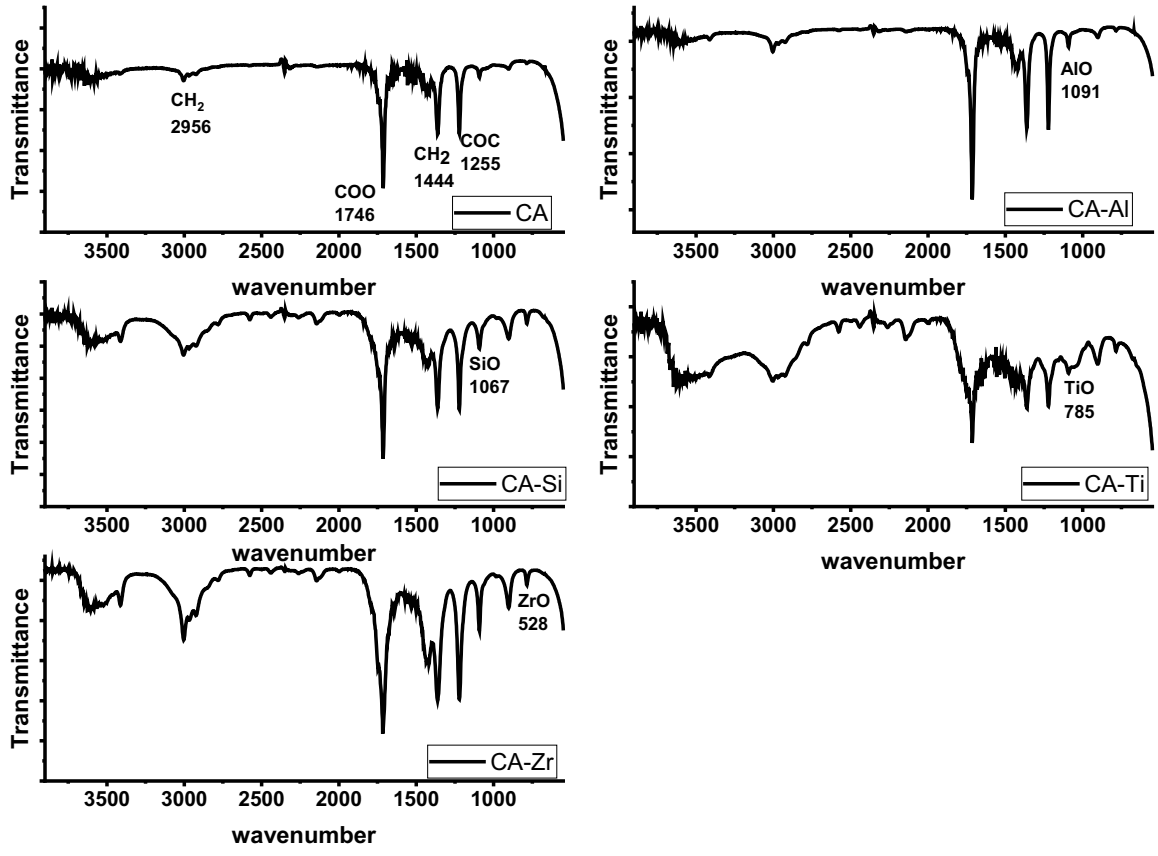

Fig. 3. FTIR spectrum of cellulose acetate based hybrids (CA, CA-Al, CA-Si, CA-Ti and CA-Zr).

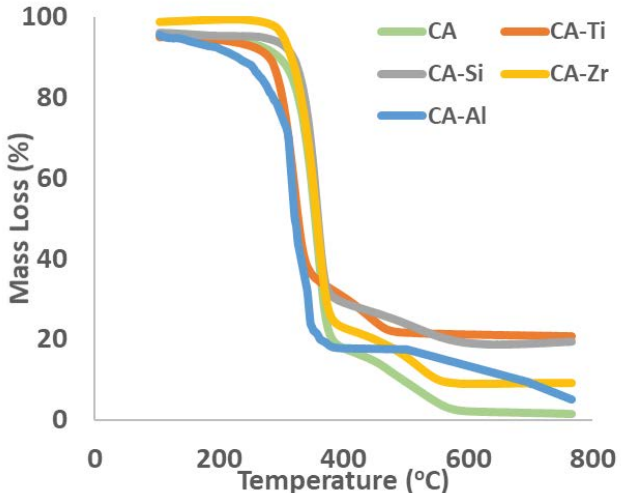

Fig. 4. TGA curve of cellulose acetate based hybrids (CA, CA-Al, CA-Si, CA-Ti).

broad exothermic peak around 330°C can be attributed to the partial pyrolysis due to fragmentation of carbonyl and carboxylic bonds from anhydrous glucoses units giving carbon or monoxide carbon [35]. The main polymer structure breaks from 350°C–370°C, which is further decomposed in 400°C–600°C region indicating further degradation and evolution of gaseous by products. The residual weights correspond to the weight at 800°C in the TGA curves. The onset temperature of 327°C in parent cellulose acetate material is typical of acetylated products. This type of increase became rapid between 200°C and 400°C due to high rate of decomposition of organic material [40]. It is noted that at higher temperatures, the hybrid materials decompose and the decomposition pattern depends upon the nature of inorganic support. The same observation is depicted from the respective residual masses of each hybrid material (Table 2)

The proposed thermal degradation patterns are presented below for the synthesized hybrids, showing the different by product is produced during their thermal degradation.

Table 1
^{1}H NMR chemical shifts for CA based hybrids and the corresponding assignments [25]

Materials	Chemical shift/ppm	Assignments*
CA	• 1.872, 1.903, 1.942, 1.981, 2.075, 2.503	• CH_3
	• 3.367, 3.682, 3. 833	• H_2, H_3'', H_2'', H_3, H_4, H_{6b}, H_5
	• 4.533, 4.607, 5.055	• H_2', H_1''
	• 5.691	• H_3'
CA-Al	• 1.878, 1.946, 1.979, 2.076, 2.506	• CH_3
	• 3.36	• H_2, H_3'', H_2'', H_3, H_4, H_{6b}, H_5
	• 4.333, 4.534, 4.664, 4.934, 5.055	• H_2', H_1''
	• 5.607	• H_3'
	• 7.187	
CA-Si	• 1.873, 1.901, 1.941, 1.979,	• CH_3
	• 2.075, 2.499, 2.504	• H_2, H_3'', H_2'', H_3, H_4, H_{6b}, H_5
	• 3.366, 3.687, 3.806, 3.954	• H_2', H_1''
	• 4.95, 4.536, 5.063	• H_3'
	• 5.649	
CA-Ti	• 1.874, 1.903, 1.943, 1.98,	• CH_3
	• 2.075, 2.503	• H_2, H_3'', H_2'', H_3, H_4, H_{6b}, H_5
	• 3.361, 3.679	• H_2', H_1''
	• 4.536, 4.6775.056, 5.658,	• H_3'
CA-Zr	• 1.877, 1.946, 1.933	• CH_3
	• 2.078, 2.507	• H_2, H_3'', H_2'', H_3, H_4, H_{6b}, H_5
	• 3.352, 3.678	• H_2', H_1''
	• 5.067, 5.454, 5.658	• H_3'

*based on the representative structure of cellulose acetate

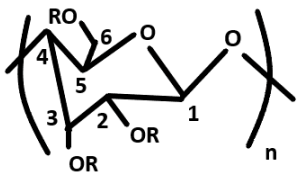

Where R = H or $COCH_3$

Table 2
Thermogravimetric data of CA based hybrids (CA, CA-Al, CA-Si, CA-Ti and CA-Zr)

Sample code	First step mass loss (%)	Second step mass loss (%)	Third step mass loss (%)	Actual residual mass (%)
CA	0.17	76	14	8.56
CA-Al	18.64	57.32	9.22	14.82
CA-Si	4.72	66.56	9	19.72
CA-Ti	4.84	58.22	14.64	20.52
CA-Zr	1.28	78.25	11.41	9.06

$$C_7H_{12}O_9Ti \rightarrow 2CO\uparrow + CO_2\uparrow + CH_3COOH + H_2O + TiO_2(\text{residue}) + C_2H_6\uparrow \quad (1)$$

$$C_7H_{12}O_9Si \rightarrow CO_2\uparrow + 2CH_3COOH + H_2O + SiO_2(\text{residue}) + C_2H_2\uparrow \quad (2)$$

$$C_7H_{12}O_9Zr \rightarrow 2CO\uparrow + CO_2\uparrow + CH_3COOH + H_2O + ZrO_2(\text{residue}) + C_2H_6\uparrow \quad (3)$$

$$2C_7H_{12}O_9Al \rightarrow 3CO\uparrow + 3CO_2\uparrow + 2CH_3COOH + 2H_2O + Al_2O_3(\text{residue}) + 2C_2H_6\uparrow \quad (4)$$

3.5. SEM and textural analysis

The morphological features of the C polymer and prepared hybrids (CA-Al, CA-Si, CA-Ti, CA-Zr) were examined by SEM images, as presented in Fig. 5. As observed from SEM images, clearly there exist morphological differences between hybrids synthesized with different inorganic moieties. The greater surface area of polymer hybrids was somewhat expected once the inorganic precursor is employed to improve the textural and morphological properties, while the organic functional polymer plays a very important role on creation of active groups cavity [44]. It is observed that with addition of each moiety, different morphologies were obtained.

CA-Zr exhibited hollow geometry with structural porosity. It is observed that the pores were hexagonal in shape and each one was surrounded by six hexagonal pores which is similar to a honeycomb, giving a homogeneously porous final network. In addition, the pores presented greater diameters, appear to be less cohesive and with lower aggregation degree, thus providing higher average pore diameter for these materials in accordance to textural data [45].

The morphological images of the CA based hybrids (CA-Al and CA-Ti) showed a rough surface and a large number of irregularly distributed agglomerates. The aggregates resemble a bunch of grapes. It can be ascribed to higher solubility of alumiuim isopropoxide in triflouroacetic acid, resulting in better blending of the polymer matrix with alumiuim fraction. There are no externally visible pores present in CA-Al hybrids, in contrast to CA-Ti morphology. The very well-defined spherical particles with fairly uniform size distribution observed for the CA-Ti, can be attributed the reason that no solvent is used, and the liquid titanium chloride is added directly added to the cellulose acetate.

The SEM images of CA-Si showed spongy structure, which upon magnification showed tiny alveoli like structures taken all together to form a very large surface area to do the work of good adsorbents. Further, the pores on the surface of sponge are clearly visible. These pores are likely to offer good adsorptive properties.

The SEM images were recorded with Hitachi SU-70 Analytical UHR FEG-SEM, and the elemental identification was performed on the surface of hybrid material by energy dispersive X-ray spectroscopy (EDX).

According to these images, change in the inorganic moiety caused the formation of largely interconnected fiber networks which may have good effect on the enhancement of the strength and pore structures.

3.6. Energy-dispersive X-ray spectroscopic analysis

Complementary information about the chemical composition of the cellulose acetate-based materials was achieved through energy-dispersive X-ray spectroscopy (EDX) on randomly selected areas of the cross sections of the hybrids and is presented as EDX spectra. It is understood that each synthesized material has a major component of C and O content; hence the major contribution to atom weight percentage is due to organic components of cellulose acetate as shown in Table 3.

In the EDX images, the characteristic elements assigned as carbon, hydrogen and oxygen can be observed. The presence of carbon and oxygen results from the chemical composition of the polymer. The new signals of silicon, titanium, aluminium and zirconium were detected in their respective hybrids. Since EDX-SEM is more sensitive for heavier atoms analysis, therefore the light atoms such as hydrogen are not detected, or they give false signals. To a close approximation, the elements C and O stands no significant variation with change in inorganic moiety.

It is noted that CA-Si hybrid materials show comparable silica and nitrogen content, indicating successful impregnation of inorganic moiety with carbon framework. These results further strengthen the preference of combination of APTMS and TEOS as inorganic moeity.

Presence of impurities in CA-Al and CA-Zr hybrids is thought to be due to the use of triflouroacetic acid. The strong acid was used to dissolve the inorganic precursors, and resulted in the detection of some other metals.

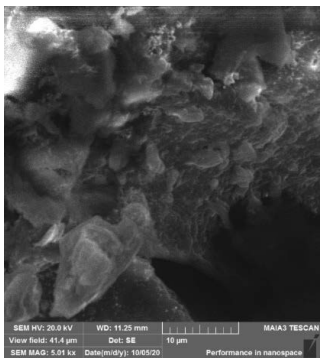

(a)

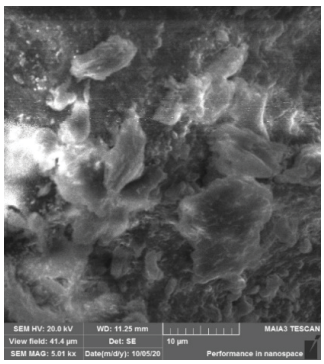

(b)

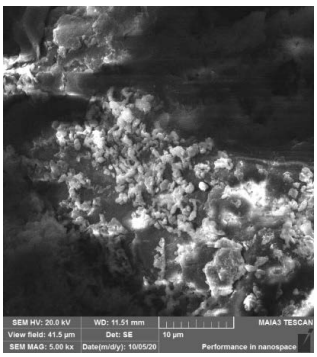

(c)

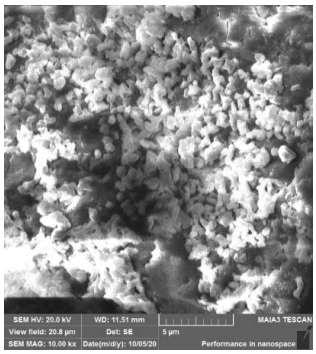

(d)

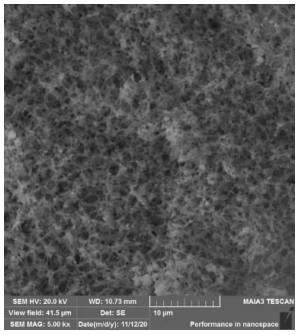

(e)

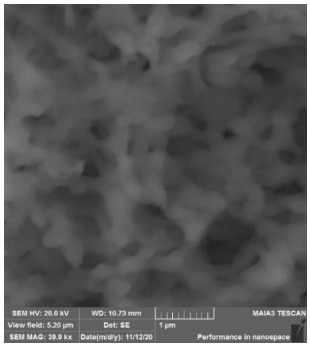

(f)

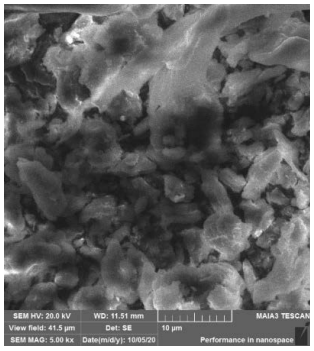

(g)

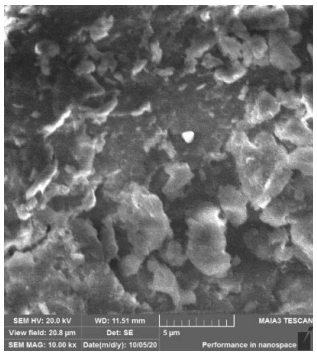

(h)

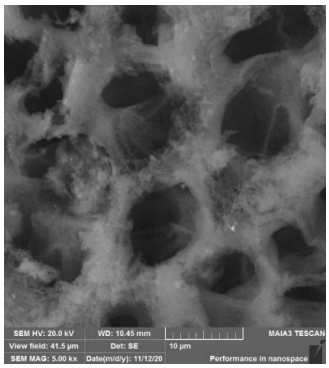

(i)

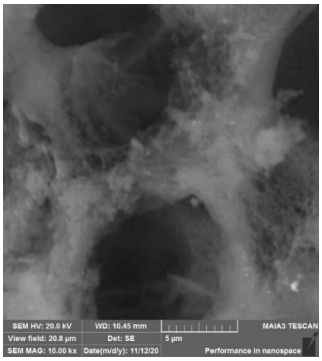

(j)

Fig. 5. SEM of cellulose acetate based hybrids (a and b) CA, (c and d) CA-Al, (e and f) CA-Si, (g and h) CA-Ti, (i and j) CA-Zr.

Table 3
Elemental composition of CA based hybrids (CA-Al, CA-Si, CA-Ti, CA-Zr)

	Atomic weight (%)							
	C	O	N	Al	Ti	Si	Zr	Impurities
CA-Al	60.75	27.17	-	1.0	–	–	–	11.08
CA-Si	62.75	25.72	0.15	–	–	11.38	–	–
CA-Ti	63.01	28.20	7.10	–	1.69	–	–	–
CA-Zr	70.85	24.47	–	0.95	–	–	0.08	3.67

3.7. Brunauer-Emmet-Teller (BET)

The textural parameters including specific surface area, BJH adsorption average pore volume, and BJH adsorption average pore diameter are obtained from nitrogen adsorption desorption presented in Table 4. It can be observed that synthesized CA based hybrids showed an increase in surface area as compared to raw cellulose acetate material in a manner CA-Si > CA-Al > CA-Ti > CA-Zr > CA. The increase in surface area is due to the incorporation of metal oxides in polymer matrix, with highest achieved in CA-Si. The comparatively higher surface area in CA-Si is due to the use of 3-aminopropyltrimethoxysilane as linker resulting in successful integration of metal on the surface. The results are in agreement with the SEM analysis, showing a spongy like structure in CA-Si, grapes like bunches on the surface of CA-Al and CA-Ti. The micropore size is doubled in CA based hybrids from 33.451 to 64–71 Å making the adsorption feasible for the Congo red molecules, which possess 18.3–22.1 Å [46].

3.8. Adsorption batch experiments

The newly synthesized CA based hybrids were used as potential adsorbents for the removal of Congo red dye. Congo red dye (CR) is a red crystalline powder with a molecular weight of 696.665 g/mol and λ_{max} = 498 (nm) by using UV Visible spectrophotometer. Adsorption batches were carried out on the synthesized hybrids to elucidate the impact of the influential parameters, that is, pH (1, 5, 7, and 11), dye concentration (0.1, 0.5, 1, 3 and 5 mg/L), contact time (0, 5, 10, 15, 30, 45, 90, 120 and 180 min), temperature (20°C, 30°C, 40°C, 50°C, 60°C) at agitation rate of 120 rpm, and 10 mg adsorbent mass. The adsorption study was performed at the selected times by withdrawing the samples followed by centrifugation and the residual dye concentration on the supernatant was determined analyzed by using a UV-Vis spectrophotometer at 498 nm and finding the values of concentration from the calibration curve method.

The efficiency capacity, Q_t (mg/g), was calculated according to a mass balance on the dye concentration using the equation:

$$Q_t = \frac{v\left(C_0 - C_t\right)}{m} \tag{5}$$

where C_0 is the initial dye concentration (mg/L), C_t is the dye concentration in solution (mg/L) at time t, V is the volume of the solution (L), and m is the mass of the adsorbent (g) [47]. The dye removal efficiency (%) of dye was also calculated using the equation:

$$\text{Removal}\left(\%\right) = \frac{\left(C_0 - C_e\right)}{C_0 \times 100} \tag{6}$$

where C_e is the concentration of dye solution (mg/L) at equilibrium [45]. Microsoft Excel program was employed for data processing.

3.9. Adsorption equilibrium experiments

Equilibrium adsorption studies were conducted at 25°C and natural pH (5.5), 50 mL of the dye solutions of different initial concentrations, from 0.1, 0.5, 1, 3 and 5 mg L^{-1}, with 10 mg of the CA based hybrids for 4 h. This time was considered enough to reach equilibrium, as maximum equilibrium was achieved at around 120 min.

3.10. Effect of contact time

The time dependent behavior of CR adsorption was examined by varying the contact time between adsorbate and adsorbent in the range of 0 min–4 h. The adsorption of CR dye is rapid at the initial stage, and reaches the steady state position, that is, at equilibrium point it slows down and almost becomes constant. The obtained results can be ascribed to the fact is that initially there are large numbers of vacant surface sites available for the adsorption, and after a lapse of time, the remaining vacant surface sites are difficult to be occupied due to repulsive forces between CR adsorbed on the surface of CA based hybrids efficient phase [48]. It is interesting to note that above mentioned behavior is applicable to all the metal based hybrids. It may be explained by the fact that each hybrid possess the same basic framework of polymer. The difference in the efficiency of the hybrids suggests that the impact of inorganic moieties on the morphology of the final hybrids as shown by SEM [49]. Overall performance of CA based hybrids on the basis of contact time follow the sequence CA-Al > CA-Si > CA-Ti > CA-Zr.

3.11. Effect of induced concentration

The effect of different initial concentrations (0.1, 0.5, 1.0, 3.0 and 5.0 ppm) of Congo red was studied on the adsorption by synthesized materials, and presented in Fig. 6. Overall, the materials showed better adsorption capacity than the raw cellulose acetate and the % removal

Table 4
BET analysis of CA based hybrids (CA, CA-Al, CA-Si, CA-Ti, CA-Zr)

Sample code	BET surface area (m^2/g)	BJH adsorption cumulative volume of pores (cm^3/g)	BJH adsorption pore diameter 4 V/A (Å)
CA	10.0713	0.006014	33.451
CA-Al	30.8504	0.046191	71.992
CA-Si	152.0968	0.17346	64.420
CA-Ti	20.9169	0.027292	68.097
CA-Zr	14.5294	0.019519	69.308

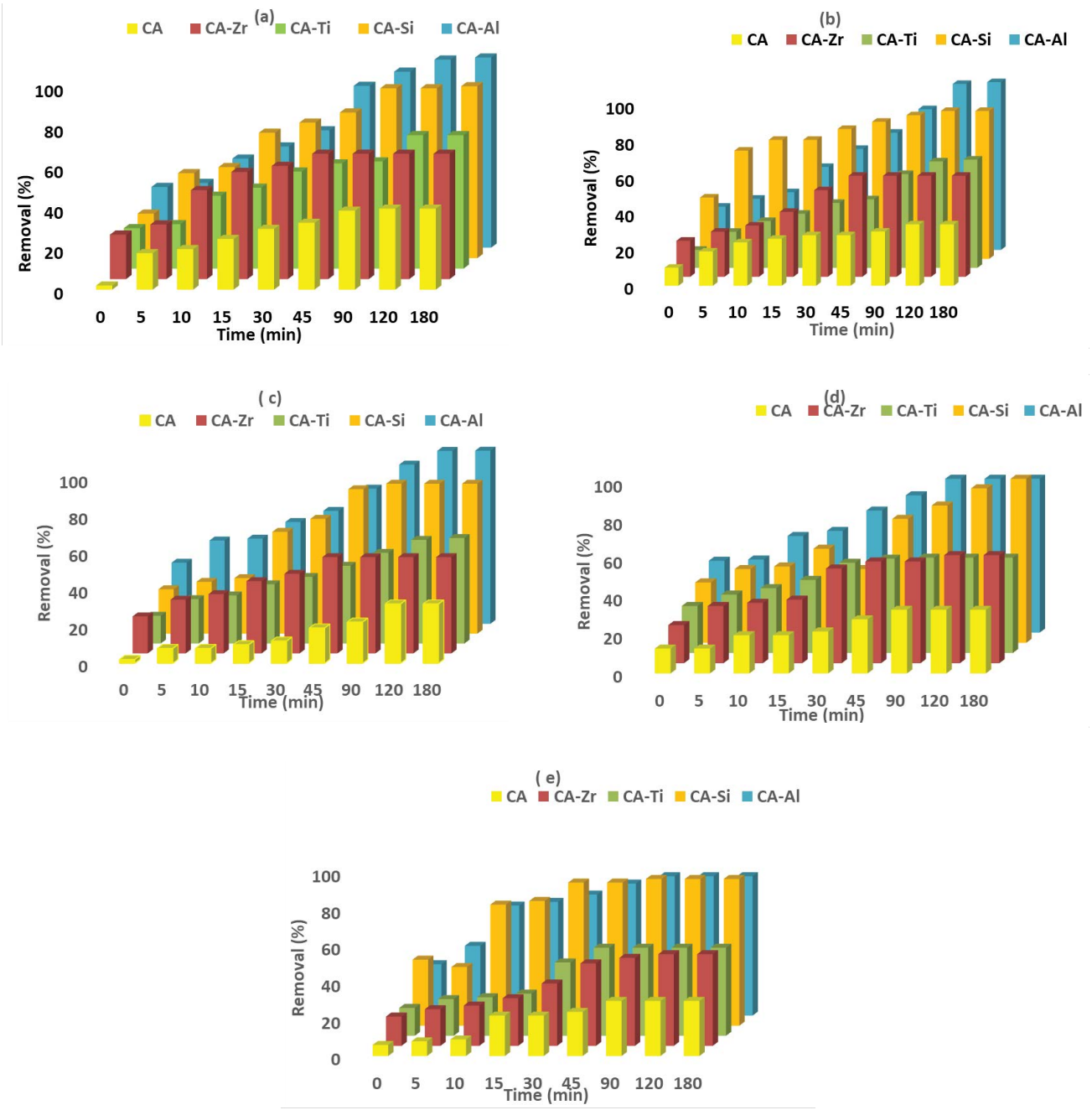

Fig. 6. Effect of concentration on % removal of Congo red by CA based hybrids (a) 0.1 ppm, (b) 0.5 ppm, (c) 1.0 ppm, (d) 3.0 ppm, and (e) 5.0 ppm

Table 5
Non-linear isotherm parameters of Langmuir, Freundlich, Temkin and DR for the removal of Congo red by CA based hybrids

Adsorbents	Slope (q_{max})	Intercept (K_L)	Slope (1/n)	n	Intercept (log k_f)	k_f (mg/g)
	Langmuir		Freundlich			
CA	0.272	0.01	0.906	1.104	0.388	2.441
CA-Al	0.198	0.001	0.743	1.347	1.389	24.489
CA-Si	0.2	0	1.109	0.902	–1.394	0.04
CA-Ti	0.2	–0.0008	1.155	0.866	–0.903	0.04
CA-Zr	0.2	0	1.154	0.866	–0.824	0.125
Adsorbents	B	B_t	A_t (L/mg)	LnQ_s	Q_s (mg/g)	K_{ad} (mol²/kJ²)
	Temkin			DR Model		
CA	1.75	1,415.931	9.061	1.322	3.752	6.2×10^{-8}
CA-Al	3.973	698.686	81.84	2.811	16.631	2.5×10^{-8}
CA-Si	4.256	582.198	32.932	2.541	12.693	3.5×10^{-8}
CA-Ti	2.8	884.959	15.756	1.932	6.902	4.6×10^{-8}
CA-Zr	2.625	943.715	14.088	1.839	6.292	4.8×10^{-8}

was decreased with increasing concentration. Equilibrium was achieved at 120 min for all the materials. Raw material had best performance at 0.1 mg/L showing 40% removal, and finally decreasing to 30% at 5.0 mg/L. Best results are achieved at 0.1 mg/L Congo red concentration (CA; 40, CA-Zr; 62, CA-Ti; 66, CA-Si; 85 and CA-Al; 94%) [50].

3.12. Effect of pH

Solution pH is an important parameter that affects the adsorption of dye molecules, because of its influence on the ionization process of dye molecules and the active binding sites of the adsorbent. The effect of the initial pH of the solution on the Congo red was assessed at different values, ranging from 1 to 11, with a contact time of 180 min, as shown in Fig. 7. The initial concentration of Congo red and amount of adsorbent was set at 1 ppm and 0.05 g, respectively, for batch test in this experiment. The results show that in general the adsorption of the dye was somewhat more efficient in the lower and neutral pH regions than in the higher pH region. The initial pH of prepared Congo red solutions was 5.5, and the raw material showed best performance at neutral pH (90%) at 15 min, however, the material failed to retain the dye with time indicating the physisorption nature and weak interaction with the dye molecules. Equilibrium is achieved in pH 1 and pH 5 at 30 min and 120 min respectively, with removal of CR as 60% and 32% respectively, where as, poor performance (2%) was shown in alkaline pH. Since the polymer provides negatively charged surface, the higher adsorption capacity observed in the lower and neutral pH region would be expected as the acidic medium would lead to an increase in hydrogen ion concentration which would then neutralize the negatively charged surface, thereby enhancing the adsorption of the negatively charged organic species because of a reduction in the forces of repulsion between adsorbent and adsorbate [51,52].

The retention power of CA-Al hybrid is better than the raw material and it showed enhanced efficiency at a wider range of pH (1–7), suggesting that the hybrid material can be applied in wide spectrum. The performance of CA-Al is expressed as pH 5 (94%) > pH 1 (90%) > pH 7 (86%) > pH 11 (25%). Similar behaviour is exhibited by CA-Si hybrids as expressed in the graph with the trend pH 1 = pH 7 (90%) > pH 5 (8%). CA-Ti hybrids show better performance at pH 1 (92%) and pH 7 (90%) as compared to initial pH (57%). Similar trend is observed by CA-Zr hybrids as pH 7 (92%) > pH 1 (90%) > pH 5 (52%). All the hybrids show poor retention ability in alkaline pH. The better performance of CA based hybrids in the acidic and neutral pH is justified by the effect of zero charge point. CR is a pH sensitive acidic dye with negative charges on its surface due to dissociation of polar sulfonic groups ($-SO_3^-$) [53]. To examine the surface charges of the CA based hybrids (as shown in Fig. 8), the point of zero charge (pH_{pzc}) was calculated. The surface charge of adsorbent is described by the ion that lies on the surface of the particle (adsorbent). It was found that the surface of synthesized hybrids was positively charged below pH 8 as compared to raw CA (pH_{pzc} = 6). From the view of the adsorbent, if the pH is below the pzc value, the surface charge of adsorbent would be positive so that the anions can be adsorbed. Conversely, if the pH is above the pzc value, the surface charge would be negative so that the cations can be adsorbed. This explains the better performance of CA based hybrids in acidic and neutral pH the surface of CA based hybrids seems to positive below pH 8, which induced electrostatic interactions between its surface and R-SO_3^-; However at high pH, the presence of excess OH^- ions competes with the dye anions for the adsorption sites. Similar results have been reported for the adsorption of CR on activated carbon [54,55]. The effect of pH variation on adsorption from model solutions became more significant as the acidity of the organic compound in aqueous solution increased: adsorption was at its strongest

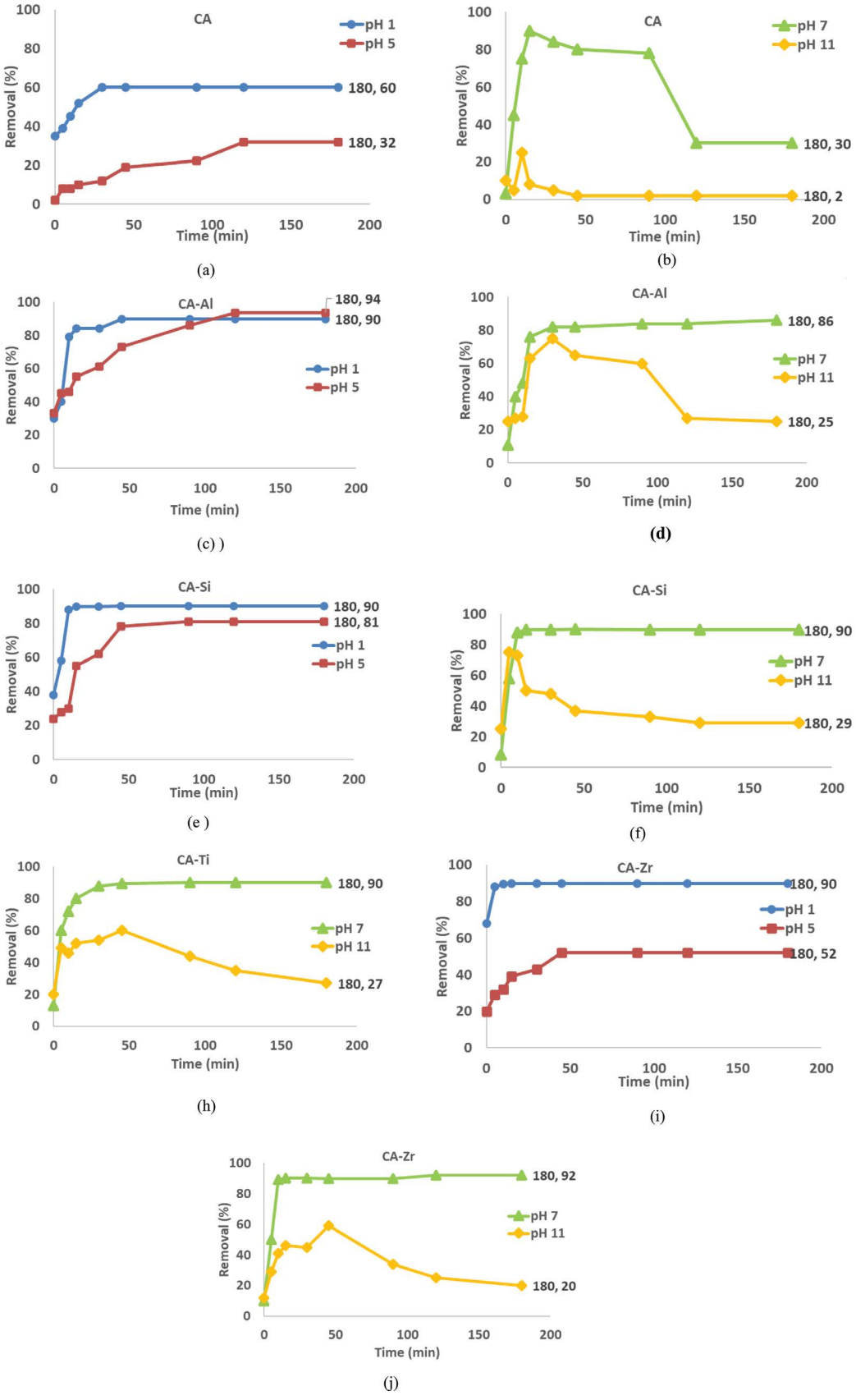

Fig. 7. Effect of pH on % removal of Congo red by CA based hybrids (a and b) CA, (c and d) CA-Al, (e and f) CA-Si, (g and h) CA-Ti, and (i and j) CA-Zr.

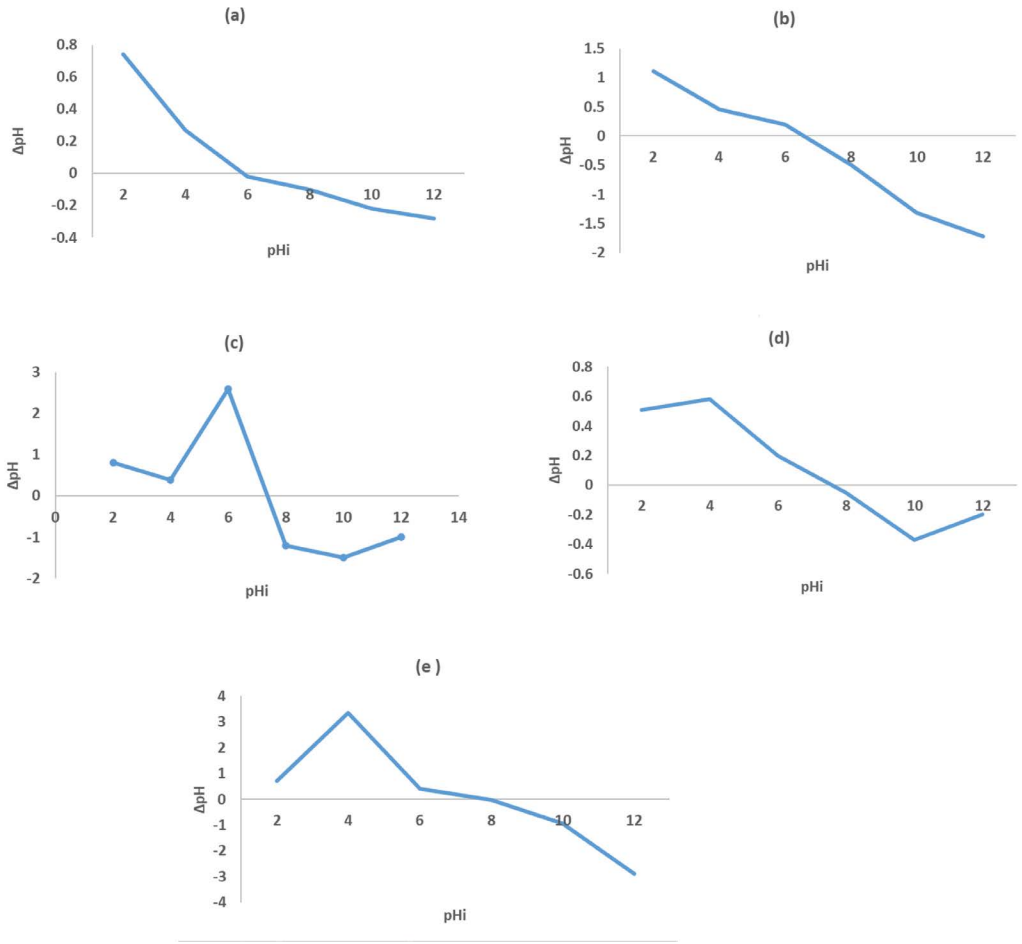

Fig. 8. Plots of ΔpH vs. pHi for salt addition method of cellulose acetate based hybrids (a) CA, (b) CA-Al, (c) CA-Si, (d) CA-Ti, and (e) CA-Zr.

in the pH region which yielded the highest proportion of undissociated molecules.

3.13. Adsorption kinetics and mechanism

Adsorption kinetics depends on the adsorbate-adsorbent interaction and system condition and has been investigated for their suitability for application in water pollution control. Two vital evaluation elements for an adsorption process operation unit are the mechanism and the reaction rate [56]. Solute uptake rate determines the residence time required for completing the adsorption reaction and can be enumerated from kinetic analysis.

Lagergren's kinetics equation has been most widely used for the adsorption of an adsorbate from an aqueous solution.

3.13.1. Lagergren's first-order

The Lagergren's first order kinetic equation was applied in its linear form:

$$\log\left(q_e - q_t\right) = \log\left(q_e\right) - \frac{k}{2.303}t \tag{7}$$

where q_t and q_e are the amounts of dye adsorbed (mg/g) at t and equilibrium time (h), respectively, and k_1 represents the first-order rate constant (h^{-1}) [57] (Fig. 9).

3.13.2. Ho's pseudo-second-order

The adsorption data were also analyzed in terms of the Ho's pseudo-second-order model [58] in the following form:

$$\frac{t}{q_t} = \frac{1}{k_2 q_e^2} + \frac{1}{q_e}t \tag{8}$$

where k_2 (g/mg h), the pseudo-second-order rate constant (Fig. 10). The initial sorption rate (h_0, mg/g h), was determined when t approaches to zero, as follows:

$$h_0 = k_2 q_e^2 \tag{9}$$

3.14. Adsorption isotherm

The purpose of studying adsorption models was not only to find a convenient mathematical expression for the relationship between adsorption capacity and adsorption

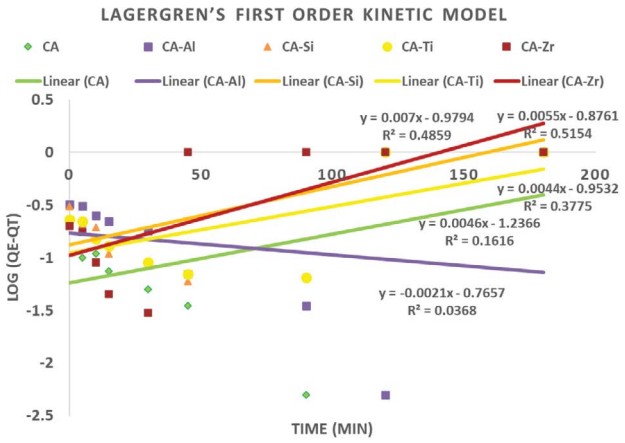

Fig. 9. Lagergren's first order kinetic model for removal of Congo red by cellulose acetate based hybrids (CA, CA-Al, CA-Si, CA-Ti and CA-Zr).

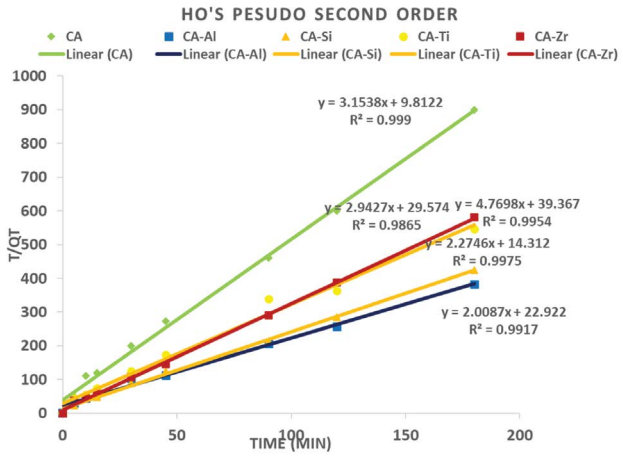

Fig. 10. Ho's second-order kinetic model for removal of Congo red by cellulose acetate based hybrids (CA, CA-Al, CA-Si, CA-Ti and CA-Zr).

conditions but also to understand the microscopic mechanism of adsorption [59]. The isotherm parameters of Langmuir, Freundlich, Temkin and DR for the removal of Congo red by CA based hybrids are tabulated in Table 5.

3.14.1. Langmuir adsorption isotherm

This describes quantitatively the formation of a monolayer adsorbate on the outer surface of the adsorbent, and after that no further adsorption takes place. Thereby, the Langmuir represents the equilibrium distribution of ions between the solid and liquid phases [60]. The Langmuir isotherm is applicable for monolayer adsorption onto a surface comprising a finite number of undistinguishable sites. The model assumes uniform energies of adsorption onto the surface and no transmigration of adsorbate in the plane of the surface. Langmuir isotherm accounts for the surface coverage by balancing the relative rates of adsorption and desorption (dynamic equilibrium) [61]. Based upon these assumptions, Langmuir represented the following equation:

$$q_e = \frac{Q_0 k_L C_e}{1 + k_L C_e} \tag{10}$$

Langmuir adsorption parameters were determined by transforming the Langmuir equation into linear form.

$$\frac{1}{q_e} = \frac{1}{Q_0} + \frac{1}{Q_0 k_L C_e} \tag{11}$$

where C_e = the equilibrium concentration of adsorbate (mg/L), q_e = the amount of dye adsorbed per gram of the adsorbent at equilibrium (mg/g), Q_0 = maximum monolayer coverage capacity (mg/g), K_L = Langmuir isotherm constant (L/mg).

The values of q_{max} and K_L were calculated from the slope and intercept of the Langmuir plot [58], as shown as Fig. 11. The essential features of the Langmuir isotherm may be expressed in terms of equilibrium parameter R_L, which is a dimensionless constant referred to as separation factor or equilibrium parameter [60].

$$R_L = \frac{1}{1 + \left(1 + k_L C_0\right)} \tag{12}$$

where C_0 = initial concentration, and K_L = Langmuir constant (the constant related to the energy of adsorption).

R_L value indicates the adsorption nature to be either unfavourable if $R_L > 1$, linear if $R_L = 1$, favourable if $0 < R_L < 1$ and irreversible if $R_L = 0$. From the data calculated in table, the R_L is greater than 1 for all the synthesized hybrids (CA-Al; 2.180 > CA; 2.018 > CA-Si; 2.000 = CA-Zr; 2.000 > CA-Ti; 1.998) indicating that equilibrium sorption is unfavourable [62–64].

In chemisorption, the amount of adsorbate required to occupy all adsorption sites on the solid surface is termed as monolayer capacity, whereas, in physisorption, it represents the amount of material required to cover the solid surface with a complete monolayer of the adsorbate in a close-packed array [65]. From this research work, the maximum monolayer coverage capacity (Q_e) from Langmuir isotherm model was determined to be maximum at the highest concentration of the dye, that is, 5 ppm. The order of decreasing Q_e is as follows: (CA-Al; 20 mg/g > CA-Si; 19 mg/g > CA-Ti; 12.5 mg/g > CA-Zr; 12.0 mg/g > CA; 7.7 mg/g), K_L (Langmuir isotherm constant) is (CA; 0.0097 L/mg > CA-Al; 0.0013 L/mg > CA-Si; 0 L/mg = CA-Zr; 0 L/mg > CA-Ti; –0.0008 L/mg), R_L (the separation factor CA-Ti) is >1 indicating that the equilibrium sorption was unfavourable and the R^2 value is 0.997, proving that the sorption data fitted well to Langmuir isotherm model.

3.14.2. Freundlich adsorption isotherm

This is commonly used to describe the adsorption characteristics for the heterogeneous surface [65]. These data often fit the empirical equation proposed by Freundlich:

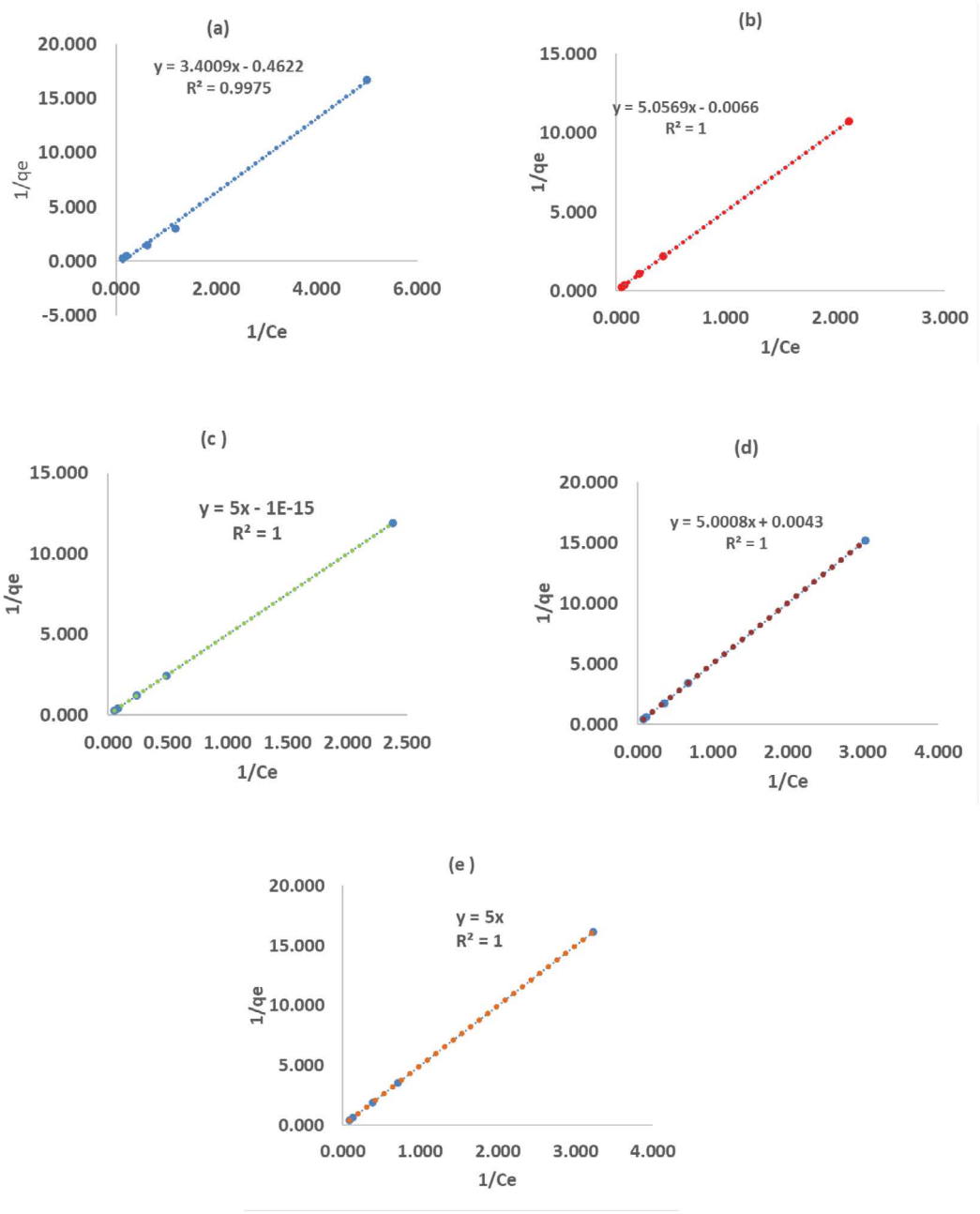

Fig. 11. Langmuir isotherm model for removal of Congo red by (a) CA, (b) CA-Al, (c) CA-Si, (d) CA-Ti, and (e) CA-Zr.

$$Q_e = k_f C^{\frac{1}{n}} \tag{13}$$

where k_f = Freundlich isotherm constant (mg/g); n = adsorption intensity; C_e = the equilibrium concentration of adsorbate (mg/L); Q_e = the amount of dye adsorbed per gram of the hybrid material at equilibrium (mg/g) [62]. Linearizing above mentioned equation, we have:

$$\log Q_e = \log k_f + \frac{1}{n}\log C_e \tag{14}$$

The constant k_f is derived from the intercept indicating the adsorption capacity, while $1/n$ (slope) is a function of the strength of adsorption in the adsorption process Fig. 12. If n = 1 then the partition between the two phases are independent of the concentration. The value of n is higher than 1 for CA; 1.104 and CA-Al; 1.347 showing that the partition between the two phases (solid and liquid) is independent of the concentrations, whereas, the values of n for remaining hybrids is less than one (CA-Si; 0.906, CA-Ti; 0.806, CA-Zr; 0.866) giving information as the separation is independent of concentration.

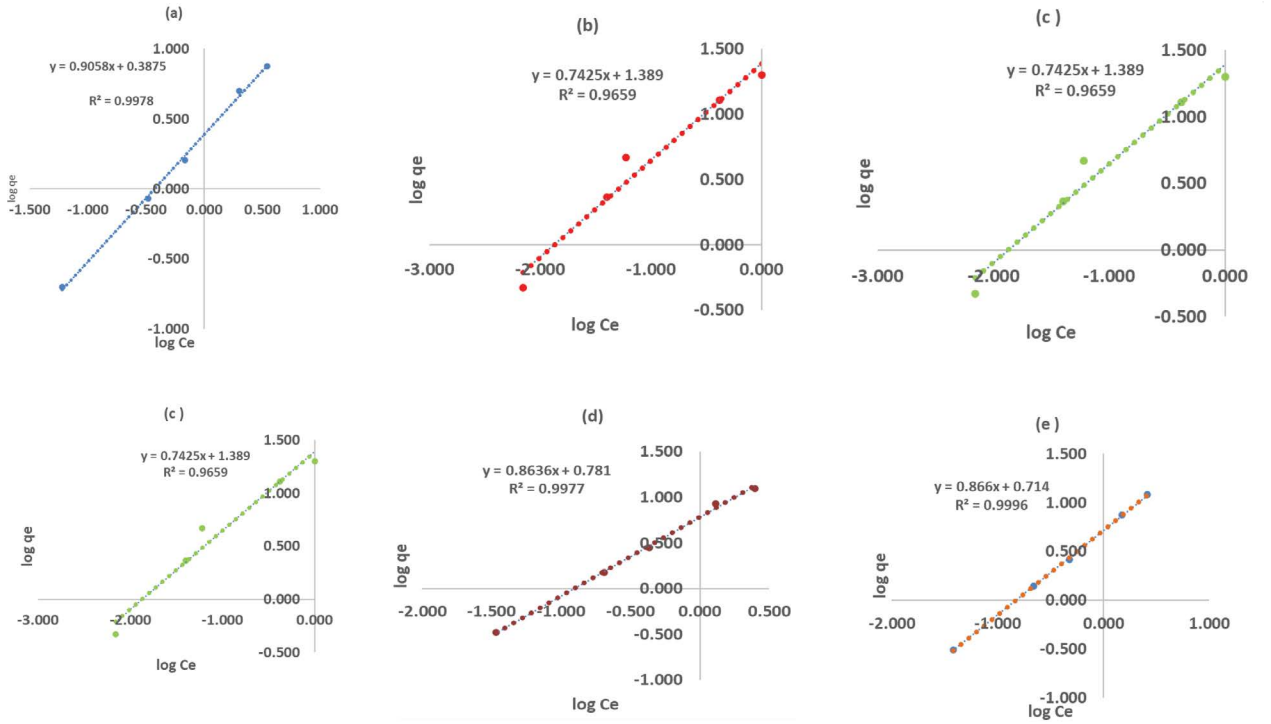

Fig. 12. Freundlich isotherm model for removal of Congo red by (a) CA, (b) CA-Al, (c) CA-Si, (d) CA-Ti, and (e) CA-Zr.

Literature shows that if value of $1/n$ is below one it indicates a normal adsorption and $1/n$ being above one indicates cooperative adsorption [66]. From the slopes of the Freundlich Isotherms, it was evident that the $1/n$ values of CA; 0.906 and CA-Al; 0.746 show normal adsorption and for the remaining hybrids it is greater than one (CA-Si; 1.109, CA-Ti; 1.155, CA-Zr; 1.154) indicating the possibility of cooperative adsorption and one (CA; 0.906 and CA-Al; 0.743) indicating the normal adsorption. On the other hand, the slope ($1/n$) of the remaining hybrids is higher than one showing the nature of adsorption as cooperative adsorption.

k_f and n are parameters characteristic of the sorbent-sorbate system, which must be determined by data fitting and whereas linear regression is generally used to determine the parameters of kinetic and isotherm models [67]. Specifically, the linear least-squares method and the linearly transformed equations have been widely applied to correlate sorption data where $1/n$ is a heterogeneity parameter, the smaller $1/n$, the greater the expected heterogeneity. The trend of heterogeneity is as follows:

CA-Al > CA > CA-Si > CA-Ti > CA-Zr. This expression reduces to a linear adsorption isotherm when $1/n$ = 1. If n lies between one and ten, this indicates a favorable sorption process [68].

3.14.3. Temkin isotherm

This isotherm is only suitable for intermediate range of adsorbate concentrations because it exhibits unrealistic asymptotic behavior and does not predict Henry's laws at low pressure [69].

The model is a semiempirical equation in which adsorption follows a pore filling mechanism [70]. It presumes a multilayer character involving Van Der Waal's forces, applicable for physical adsorption processes, and is a fundamental equation that qualitatively describes the adsorption of gases and vapours on microporous sorbents [60].

This isotherm contains a factor that explicitly taking into the account of adsorbent–adsorbate interactions. By ignoring the extremely low and large value of concentrations, the model assumes that heat of adsorption (function of temperature) of all molecules in the layer would decrease linearly rather than logarithmic with coverage [70]. It is usually applied to differentiate between physical and chemical adsorption [71].

As implied in the equation, its derivation is characterized by a uniform distribution of binding energies (up to some maximum binding energy) by plotting the quantity sorbed q_e against $\ln C_e$ and the constants were determined from the slope and intercept. The model is given by the following equation [65].

$$q_e = \frac{RT}{b}\ln\left(A_T C_e\right) \tag{15}$$

$$q_e = \frac{RT}{b_T}\ln A_T + \left(\frac{RT}{b}\right)\ln C_e \tag{16}$$

$$B = \frac{RT}{b_T} \tag{17}$$

$$q_e = B\ln A_T + B\ln C_e \tag{18}$$

where A_T = Temkin isotherm equilibrium binding constant (L/g); b_T = Temkin isotherm constant; R = universal

gas constant (8.314 J/mol/K); T = Temperature at 298 K; B = Constant related to heat of sorption (J/mol). From the Temkin isotherm plots shown below, the values of B were calculated from the slopes, and b_T was determined by using the formula shown below:

$$b_T = \frac{RT}{B} \tag{19}$$

were estimated (Fig. 13). A_T = 1.075 L/g, B = 25.34 J/mol which is an indication of the heat of sorption indicating a physical adsorption process and the R^2 = 0.62.

3.14.4. Dubinin–Radushkevich isotherm model

Dubinin–Radushkevich isotherm is generally useful to explain the adsorption mechanism with a Gaussian energy distribution onto a heterogeneous surface [58]. The model has often successfully fitted high solute activities CA-Ti and the intermediate range of concentrations data well:

$$q_e = (q_s)\exp\left(-k_{\text{ad}}\varepsilon^2\right) \tag{20}$$

$$\ln q_e = \ln(q_s) - \left(K_{\text{ad}}\varepsilon^2\right) \tag{21}$$

where q_e, q_s, K_{ad}, are q_e = amount of adsorbate in the adsorbent at equilibrium (mg/g); q_s = theoretical isotherm saturation capacity (mg/g); K_{ad} = Dubinin–Radushkevich isotherm constant (mol²/kJ²) and ε = Dubinin–Radushkevich isotherm constant. The approach was usually applied to distinguish the physical and chemical adsorption of metal ions with its mean free energy, E per molecule of adsorbate (for removing a molecule from its location in the sorption space to the infinity) can be computed by the relationship [65].

$$E = \frac{1}{\sqrt{2B_{\text{DR}}}} \tag{22}$$

where BDR is denoted as the isotherm constant. Meanwhile, the parameter can be calculated as:

$$\varepsilon = RT\ln\left[1+\frac{1}{c_e}\right] \tag{23}$$

where R, T and C_e represent the gas constant (8.314 J/mol K), absolute temperature (K) and adsorbate equilibrium concentration (mg/L), respectively [72]. The constant such as q_s and K_{ad} were determined from the appropriate plot using above equation. From the linear plot of DRK model) (Fig. 14), q_s was determined and found to be (CA; 3.752, CA-Al; 16.631, CA-Si; 12.693, CA-Ti; 6.902, CA-Zr; 6.292 mg/g, the mean free energy, E = 0.7 KJ/mol indicating a physiosorption process and the R^2 = 0.818 (CA), 00.974 (CA-Al), 0.921 (CA-Si), 0.817 (CA-Ti), 0.857 (CA-Zr).

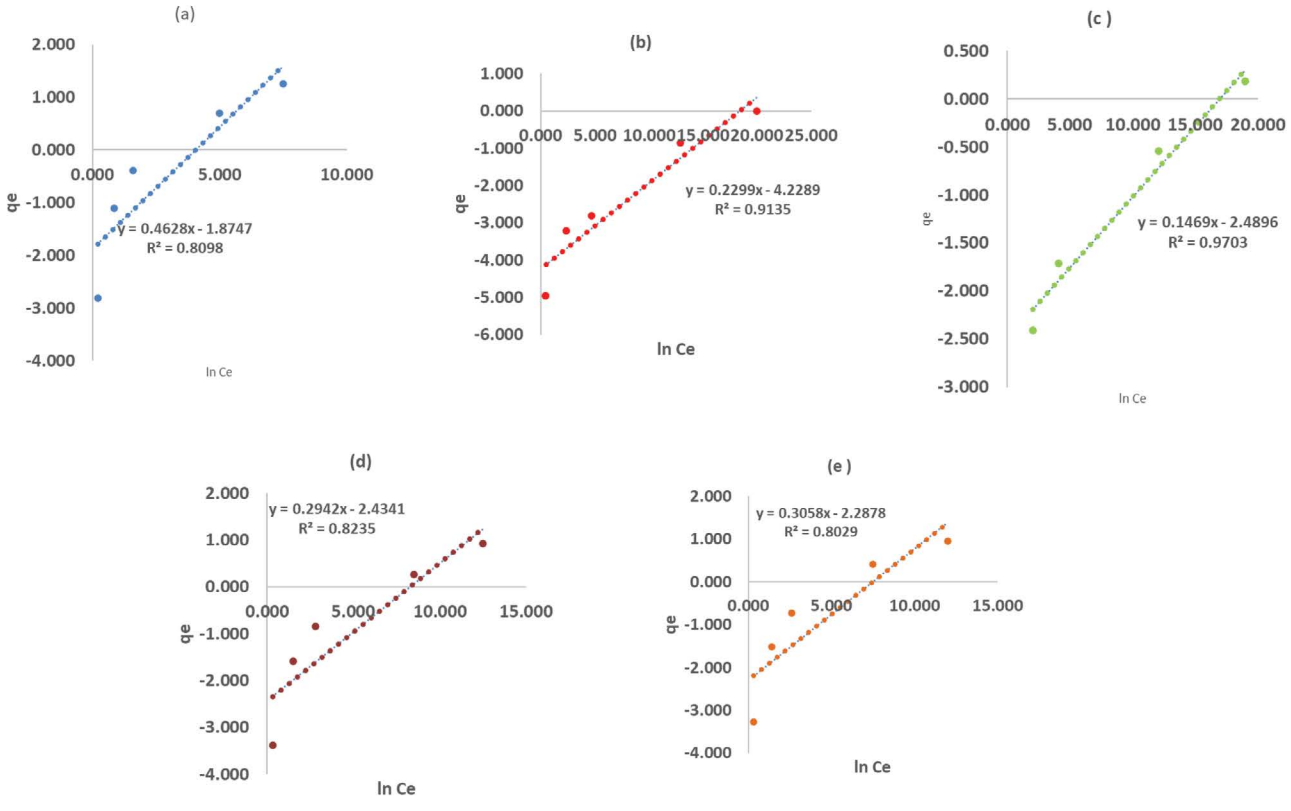

Fig. 13. Temkin isotherm model for removal of Congo red by (a) CA, (b) CA-Al, (c) CA-Si, (d) CA-Ti, and (e) CA-Zr.

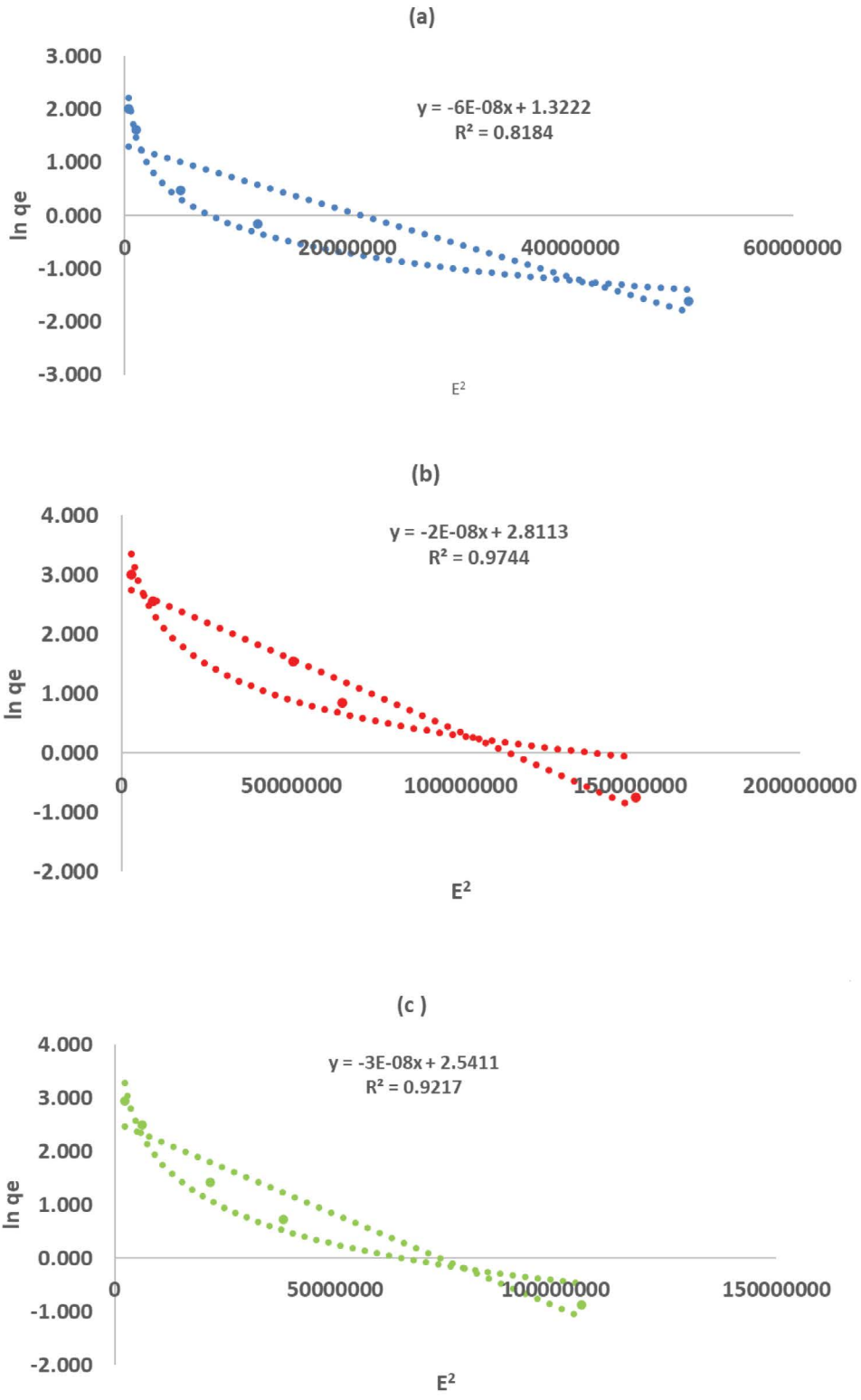

Fig. 14. DR Isotherm model for removal of Congo red by (a) CA, (b) CA-Al, (c) CA-Si

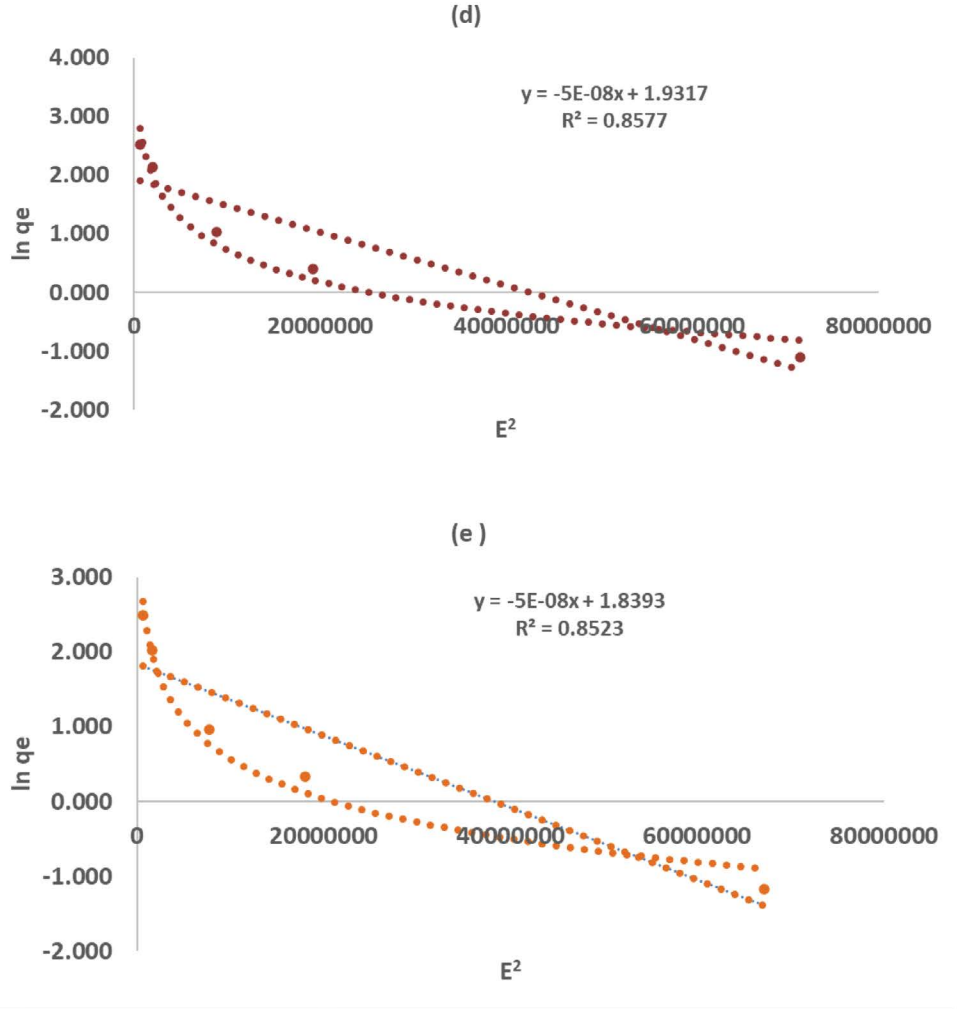

Fig. 14. DR Isotherm model for removal of Congo red by (d) CA-Ti, and (e) CA-Zr.

4. Proposed adsorption mechanism

Congo red is an elongated, flat molecule with bilateral symmetry. It possesses three bonding sites in a molecule for van der Waal's forces including sulfonic acids, amines and a large conjugated system. The distance between ionic bonding sites ranges from 18.3 to 22.1 Å, with lowermost hydrogen atoms on the amines 14.6 Å apart [46].

The present analysis of BET shows an increase in surface area, micropore volume and diameter, enhancing the binding of Congo red molecules on to the surface of synthesized hybrids more efficient in the synthesized hybrids. Furthermore, the pzc values indicate that the surface is positively charged below pH 8, facilitating the removal of Congo red (anionic dye).

5. Conclusions

Cellulose acetate based hybrids were synthesized by using a facile approach. The elucidation data showed formation of an amorphous agglomerates on the cellulose acetate surface, with the London type nature of interaction. The hybrids were subjected to the removal studies of Congo red dye from model solutions It was concluded that the hybrids performed extremely well at a wider range of pH (1–7) with 0.1 ppm dye concentration, 10 mg dose/0.05 L dye solution, which is in agreement with the pzc. Kinetic studies reveal that the adsorption follows pseudo-second-order reaction mechanism. The order of decreasing Q_e is as follows: (CA-Al; 20 mg/g > CA-Si; 19 mg/g > CA-Ti; 12.5 mg/g > CA-Zr; 12.0 mg/g > CA; 7.7 mg/g), K_L (Langmuir isotherm constant) is (CA; 0.0097 L/mg > CA-Al; 0.0013 L/mg > CA-Si; 0 L/mg = CA-Zr; 0 L/mg > CA-Ti; –0.0008 L/mg), R_L (the separation factor) is >1 indicating that the equilibrium sorption was unfavourable and the R^2 value is 0.997 for parent material and 1 for each of the synthesized hybrids, proving that the sorption data fitted well to Langmuir isotherm model.

From the slopes of the Freundlich isotherms, it was evident that the 1/n values of CA; 0.906 and CA-Al; 0.746 show normal adsorption and for the remaining hybrids it is greater than one (CA-Si; 1.109, CA-Ti; 1.155, CA-Zr; 1.154) indicating the possibility of cooperative adsorption.

From the linear plot of DRK model, q_s was determined and found to be (CA; 3.752, CA-Al; 16.631, CA-Si; 12.693, CA-Ti; 6.902, CA-Zr; 6.292 mg/g, the mean free energy, E = 0.7 kJ/mol indicating a physiosorption process and the R^2 = 0.818 (CA), 00.974 (CA-Al), 0.921 (CA-Si), 0.817 (CA-Ti), 0.857 (CA-Zr). We believe that the approach presented herein can provide a convenient way to synthesize sustainable and inexhaustible new materials that can be used as potential adsorbent for the removal of wide range of organic dyes from wastewater.

Declaration

Author contributions

The authors contribute for the experimental design and activities, manuscript writing and editing and approved the final manuscript.

Funding

This research did not receive any specific grant from funding agencies in the public, commercial or not for profit sector. The research work was carried out by the departmental funding allocated for research.

Data availability

The detailed information is described in the body of the manuscript.

Acknowledgment

The authors express their appreciation to the department of Environmental Sciences, Fatima Jinnah Women University, Rawalpindi.

References

[1] M.N. Iqbal, A. Ashraf, Environmental pollution: heavy metals removal from water sources, Int. J. Altern. Fuels Energy, 2 (2018) 14–15.

[2] M.N. Rashed, Adsorption Technique for the Removal of Organic Pollutants from Water and Wastewater, M. Nageeb Rashed, Ed., Organic Pollutants – Monitoring, Risk and Treatment, IntechOpen, 2013, pp. 167–194, doi: 10.5772/54048. Available from: https://www.intechopen.com/chapters/42059

[3] A.M. Mahmoud, F.A. Ibrahim, S.A. Shaban, N.A. Youssef, Adsorption of heavy metal ion from aqueous solution by nickel oxide nano catalyst prepared by different methods, Egypt. J. Pet., 24 (2015) 27–35.

[4] L. Novikova, L. Belchinskaya, Adsorption of Industrial Pollutants by Natural and Modified Aluminosilicates, G.M. do Nascimento, Ed., Clays, Clay Minerals and Ceramic Materials Based on Clay Minerals, IntechOpen, 2016, doi: 10.5772/61678.

[5] G. Lligadas, J.C. Ronda, M. Galià, V. Cádiz, Renewable polymeric materials from vegetable oils: a perspective, Mater. Today, 16 (2013) 337–343.

[6] L. Wang, X.-L. Wu, W.-H. Xu, X.-J. Huang, J.-H. Liu, A.-W. Xu, Stable organic–inorganic hybrid of polyaniline/α-zirconium phosphate for efficient removal of organic pollutants in water environment, ACS Appl. Mater. Interfaces, 4 (2012) 2686–2692.

[7] Y. Pang, G. Zeng, L. Tang, Y. Zhang, Y. Liu, X. Lei, G. Xie, PEI-grafted magnetic porous powder for highly effective adsorption of heavy metal ions, Desalination, 281 (2011) 278–284.

[8] E. Repo, J.K. Warchoł, A. Bhatnagar, M. Sillanpää, Heavy metals adsorption by novel EDTA-modified chitosan–silica hybrid materials, J. Colloid Interface Sci., 358 (2011) 261–267.

[9] E.B. Simsek, D. Duranoglu, U. Beker, Heavy metal adsorption by magnetic hybrid-sorbent: an experimental and theoretical approach, Sep. Sci. Technol., 47 (2012) 1334–1340.

[10] N. Zaitseva, V. Zaitsev, A. Walcarius, Chromium(VI) removal via reduction–sorption on bi-functional silica adsorbents, J. Hazard. Mater., 250 (2013) 454–461.

[11] B. Samiey, C.-H. Cheng, J. Wu, Organic-inorganic hybrid polymers as adsorbents for removal of heavy metal ions from solutions: a review, Materials, 7 (2014) 673–726.

[12] L. Mercier, T.J. Pinnavaia, Heavy metal ion adsorbents formed by the grafting of a thiol functionality to mesoporous silica molecular sieves: factors affecting Hg(II) uptake, Environ. Sci. Technol., 32 (1998) 2749–2754.

[13] B. Pan, B. Pan, W. Zhang, L. Lv, Q. Zhang, S. Zheng, Development of polymeric and polymer-based hybrid adsorbents for pollutants removal from waters, Chem. Eng. J., 151 (2009) 19–29.

[14] M. Tavakolian, S.M. Jafari, T.G. van de Ven, A review on surface-functionalized cellulosic nanostructures as biocompatible antibacterial materials, Nano-Micro Lett., 12 (2020) 1–23.

[15] H. Kargarzadeh, M. Mariano, J. Huang, N. Lin, I. Ahmad, A. Dufresne, S. Thomas, Recent developments on nanocellulose reinforced polymer nanocomposites: a review, Polymer, 132 (2017) 368–393.

[16] H.P.S. Khalil, F. Jummaat, E.B. Yahya, N.G. Olaiya, A.S. Adnan, M. Abdat, A.B. Suriani, A review on micro-to nanocellulose biopolymer scaffold forming for tissue engineering applications, Polymers, 12 (2020) 2043, doi: 103390/polym12092043.

[17] K. Khoshnevisan, H. Maleki, H. Samadian, S. Shahsavari, M.H. Sarrafzadeh, B. Larijani, M.R. Khorramizadeh, Cellulose acetate electrospun nanofibers for drug delivery systems: applications and recent advances, Carbohydr. Polym., 198 (2018) 131–141.

[18] E.A. de Campos, S.D. de Campos, A.A. Roos, B.V. de Souza, J.M. Schneider, M.B. Uliana, R.C. de Oliveira, Titanium dioxide dispersed on cellulose acetate and its application in methylene blue photodegradation, Polym. Polym. Compos., 21 (2013) 423–430.

[19] A. Tabernero, S. Cardea, Supercritical carbon dioxide techniques for processing microbial exopolysaccharides used in biomedical applications, Mater. Sci. Eng., C, 112 (2020) 110940, doi: 101016/jmsec2020110940.

[20] S. Pavlidou, C.D. Papaspyrides, A review on polymer–layered silicate nanocomposites, Prog. Polym. Sci., 33 (2008) 1119–1198.

[21] X. Yang, J. Ma, J. Ling, N. Lin, D. Wang, F. Yue, S. Xu, Cellulose acetate-based SiO_2/TiO_2 hybrid microsphere composite aerogel films for water-in-oil emulsion separation, Appl. Surf. Sci., 435 (2018) 609–616.

[22] G. Splendore, E.V. Benvenutti, Y.V. Kholin, Y. Gushikem, Cellulose acetate-Al_2O_3 hybrid material coated with N-Propyl-1,4-diazabicyclo [2.2.2] octane chloride: preparation, characterization and study of some metal halides adsorption from ethanol solution, J. Braz. Chem. Soc., 16 (2005) 147–152.

[23] W.F. Tan, S.J. Lu, F. Liu, X.H. Feng, J.Z. He, Determination of the point of zero charge of manganese oxides with different methods including an improved salt titration method, J. Soil Sci., 173 (2008) 277–286.

[24] T. Mahmood, M.T. Saddique, A. Naeem, P. Westerhoff, S. Mustafa, A. Alum, Comparison of different methods for the point of zero charge determination of NiO, Ind. Eng. Chem. Res., 50 (2011) 10017–10023.

[25] A.M. Das, A.A. Ali, M.P. Hazarika, Synthesis and characterization of cellulose acetate from rice husk: eco-friendly condition, Carbohydr. Polym., 112 (2014) 342–349.

[26] A.H. Basta, W.M. Hosny, Dioxouranium (VI) complexes with cellulose acetate, Polym. Degrad. Stab., 60 (1998) 239–245.

[27] T. Heinze, K. Rahn, The first report on a convenient synthesis of novel reactive amphiphilic polysaccharides, Macromol. Rapid Commun., 17 (1996) 675–681.

[28] L. Mao, A.M. Ritcey, Preparation of cellulose derivatives containing carbazole chromophore, J. Appl. Polym. Sci., 74 (1999) 2764–2772.
[29] M. Kamal, E.M. Abdelrazek, N.M. Sellow, A.M. Abdelghany, Synthesis and optimization of novel chitosan/cellulose acetate natural polymer membrane for water treatment, J. Adv. Phys., 14 (2018) 5303–5311.
[30] A. Günay, E. Arslankaya, I. Tosun, Lead removal from aqueous solution by natural and pretreated clinoptilolite: adsorption equilibrium and kinetics, J. Hazard. Mater., 146 (2007) 362–371.
[31] M.H. Alotaibi, G.A. El-Hiti, H. Hashim, A.S. Hameed, D.S. Ahmed, E. Yousif, SEM analysis of the tunable honeycomb structure of irradiated poly(vinyl chloride) films doped with polyphosphate, Heliyon, 4 (2018) e01013.
[32] A.M. Das, A. Ali, M.P. Hazarika, Synthesis and characterization of cellulose acetate from rice husk: eco-friendly condition, Carbohydr. Polym., 112 (2014) 342–349.
[33] W. Hu, S. Chen, Q. Xu, H. Wang, Solvent-free acetylation of bacterial cellulose under moderate conditions, Carbohydr. Polym., 83 (2011) 1575–1581.
[34] J. Casarin, A.C. Gonçalves Jr., M.G. Segatelli, C.R.T. Tarley, Poly(methacrylic acid)/SiO_2/Al_2O_3 based organic-inorganic hybrid adsorbent for adsorption of imazethapyr herbicide from aqueous medium, React. Funct. Polym., 121 (2017) 101–109.
[35] H.S. Barud, A.M. de Araújo Júnior, D.M. Santos, R.M. de Assunção, C.S. Meireles, D.A. Cerqueira, S.J. Ribeiro, Thermal behavior of cellulose acetate produced from homogeneous acetylation of bacterial cellulose, Thermochim. Acta, 471 (2008) 61–69.
[36] N.R. Aswathy, A.K. Palai, A. Ramadoss, S. Mohanty, S.K. Nayak, Fabrication of cellulose acetate-chitosan based flexible 3D scaffold-like porous membrane for supercapacitor applications with PVA gel electrolyte, Cellulose, 27 (2020) 3871–3887.
[37] C. Hu, J. Deng, Y. Zhao, L. Xia, K. Huang, S. Ju, N.N. Xiao, A novel core–shell magnetic nano-sorbent with surface molecularly imprinted polymer coating for the selective solid phase extraction of dimetridazole, Food Chem., 158 (2014) 366–373.
[38] I.A. Rahman, V. Padavettan, Synthesis of silica nanoparticles by sol-gel: size-dependent properties, surface modification, and applications in silica-polymer nanocomposites—a review, J. Nanomater., 2012 (2012) 8–16.
[39] L.D. Prola, L. Bach-Toledo, J. Schultz, A.S. Mangrich, P.G. Peralta-Zamora, Synthesis, characterization, and synergic photocatalytic activity of amorphous TiO_2/chitosan carbon microspheres, J. Braz. Chem. Soc., 31 (2020) 1306–1316.
[40] W. Qiu, Y. Luo, F. Chen, Y. Duo, H. Tan, Morphology and size control of inorganic particles in polyimide hybrids by using SiO_2–TiO_2 mixed oxide, Polymer, 44 (2003) 5821–5826.
[41] W.A. Siddiqui, S.A. Khan, Synthesis, characterization and ion-exchange properties of a new and novel 'organic–inorganic' hybrid cation-exchanger: poly(methyl methacrylate) Zr(IV) phosphate, Colloids Surf., A, 295 (2007) 193–199.
[42] V.K. Gupta, D. Pathania, P. Singh, B.S. Rathore, P. Chauhan, Cellulose acetate–zirconium(IV) phosphate nano-composite with enhanced photo-catalytic activity, Carbohydr. Polym., 95 (2013) 434–440.
[43] H. Asai, H. Nitani, F. Nishimura, S. Yonezawa, K. Nakane, Structural analysis of cellulose acetate and zirconium alkoxide hybrid fibres, RSC Adv., 6 (2016) 45858–45863.
[44] D.N. Clausen, I.M.R. Pires, C.R.T. Tarley, Improved selective cholesterol adsorption by molecularly imprinted poly(methacrylic acid)/silica (PMAA–SiO_2) hybrid material synthesized with different molar ratios, Mater. Sci. Eng., C, 44 (2014) 99–108.
[45] R.A. Caruso, J.H. Schattka, Cellulose acetate templates for porous inorganic network fabrication, J. Adv. Mater., 12 (2000) 1921–1923.
[46] R.W. Dapson, Amyloid from a histochemical perspective. A review of the structure, properties and types of amyloid, and a proposed staining mechanism for Congo red staining, Biotech. Histochem., 93 (2018) 543–556.
[47] Y. Azeh, D.O. Adetitun, G.A. Olatunji, F.A. Adekola, Application of cellulose acetate reinforced nanocomposite fluorescence film as filter and bio-packaging material with antibacterial properties, Ann. Sci. Technol., 5 (2020) 45–55.
[48] T. Taher, D. Rohendi, R. Mohadi, A. Lesbani, Congo red dye removal from aqueous solution by acid-activated bentonite from sarolangun: kinetic, equilibrium, and thermodynamic studies, Arab J. Basic Appl. Sci., 26 (2019) 125–136.
[49] K. Zare, H. Sadegh, R. Shahryari-Ghoshekandi, B. Maazinejad, V. Ali, I. Tyagi, V.K. Gupta, Enhanced removal of toxic Congo red dye using multi walled carbon nanotubes: kinetic, equilibrium studies and its comparison with other adsorbents, J. Mol. Liq., 212 (2015) 266–271.
[50] W. Qiu, Y. Luo, F. Chen, Y. Duo, H. Tan, Morphology and size control of inorganic particles in polyimide hybrids by using SiO_2–TiO_2 mixed oxide, Polymer, 44 (2003) 5821–5826.
[51] S.H. Kim, P.P. Choi, Enhanced Congo red dye removal from aqueous solutions using iron nanoparticles: adsorption, kinetics, and equilibrium studies, Dalton Trans., 46 (2017) 15470–15479.
[52] S. Wong, N. Abd Ghafar, N. Ngadi, F.A. Razmi, I.M. Inuwa, R. Mat, N.A.S. Amin, Effective removal of anionic textile dyes using adsorbent synthesized from coffee waste, Sci. Rep., 10 (2020) 1–13.
[53] Z.L. Yaneva, N.V. Georgieva, Insights into Congo red adsorption on agro-industrial materials - spectral, equilibrium, kinetic, thermodynamic, dynamic and desorption studies. A review, Int. Rev. Chem. Eng. (I.RE.CH.E.), 4 (2012) 127–146.
[54] S. Liu, Y. Ding, P. Li, Adsorption of the anionic dye Congo red from aqueous solution onto natural zeolites modified with N,N-dimethyl dehydroabietylamine oxide, Chem. Eng. J., 248 (2014) 135–144.
[55] M.K. Purkait, A. Maiti, S. DasGupta, Removal of Congo red using activated carbon and its regeneration, J. Hazard. Mater., 145 (2007) 287–295.
[56] N.A. Fathy, O.I. El-Shafey, L.B. Khalil, Effectiveness of alkali-acid treatment in enhancement the adsorption capacity for rice straw: the removal of methylene blue dye, Int. Scholarly Res. Notices, 2013 (2013) 1–15, doi: 101155/2013/208087.
[57] S. Iftekhar, D.L. Ramasamy, V. Srivastava, M.B. Asif, M. Sillanpää, Understanding the factors affecting the adsorption of Lanthanum using different adsorbents: a critical review, Chemosphere, 204 (2018) 413–430.
[58] S.K. Lagergren, About the theory of so-called adsorption of soluble substances, Sven. Vetenskapsakad. Handingar, 24 (1898) 1–39.
[59] Y.S. Ho, G. McKay, Pseudo-second-order model for sorption processes, Process Biochem., 34 (1999) 451–465.
[60] Q. Hu, Z. Zhang, Application of Dubinin–Radushkevich isotherm model at the solid/solution interface: a theoretical analysis, J. Mol. Liq., 277 (2019) 646–648.
[61] A.O. Dada, A.P. Olalekan, A.M. Olatunya, O. Dada, Langmuir, Freundlich, Temkin and Dubinin–Radushkevich isotherms studies of equilibrium sorption of Zn^{2+} unto phosphoric acid modified rice husk, IOSR J. Appl. Chem., 3 (2012) 38–45.
[62] H. Xiyili, S. Çetintaş, D. Bingöl, Removal of some heavy metals onto mechanically activated fly ash: modeling approach for optimization, isotherms, kinetics and thermodynamics, Process Saf. Environ. Prot., 109 (2017) 288–300.
[63] H.K. Boparai, M. Joseph, D.M. O'Carroll, Kinetics and thermodynamics of cadmium ion removal by adsorption onto nano zerovalent iron particles, J. Hazard. Mater., 186 (2011) 458–465.
[64] N. Ayawei, A.N. Ebelegi, D. Wankasi, Modelling and interpretation of adsorption isotherms, J. Chem., 2017 (2017) 3039817, doi: 101155/2017/3039817.
[65] M. El Haddad, R. Slimani, R. Mamouni, S. ElAntri, S. Lazar, Removal of two textile dyes from aqueous solutions onto calcined bones, J. Assoc. Arab Univ. Basic Appl. Sci., 14 (2013) 51–59.
[66] F. Togue Kamga, Modeling adsorption mechanism of paraquat onto Ayous (*Triplochiton scleroxylon*) wood sawdust, Appl. Water Sci., 9 (2019) 1, doi: 101007/s13201-018-0879-3.

[67] G. De la Rosa, A.B.P. Reynel-Ávila, I. Cano-Rodríguez, C. Velasco-Santos, Martínez-Hernandez, Al Reciclagem de penas de aves de capoeira para remoção de Pb de águas residuais: estudos cinéticos e de equilíbrio, Int. J. Chem. Biol. Eng., 1 (2008) 185–193.
[68] S. Goldberg, Equations and models describing adsorption processes in soils, Chem. Processes Soil, 8 (2005) 489–517.
[69] A. Dąbrowski, Adsorption—from theory to practice, Adv. Colloid Interface Sci., 93 (2001) 135–224.
[70] N. Ayawei, A.T. Ekubo, D. Wankasi, E.D. Dikio, Adsorption of Congo red by Ni/Al-CO_3: equilibrium, thermodynamic and kinetic studies, Orient. J. Chem., 31 (2015) 1307, doi: 1013005/ojc/310307.
[71] I. Langmuir, The adsorption of gases on plane surfaces of glass, mica and platinum, J. Am. Chem. Soc., 40 (1998) 1361–1403.
[72] K.Y. Foo, B.H. Hameed, Insights into the modeling of adsorption isotherm systems, Chem. Eng. J., 156 (2010) 2–10.

Supplementary information

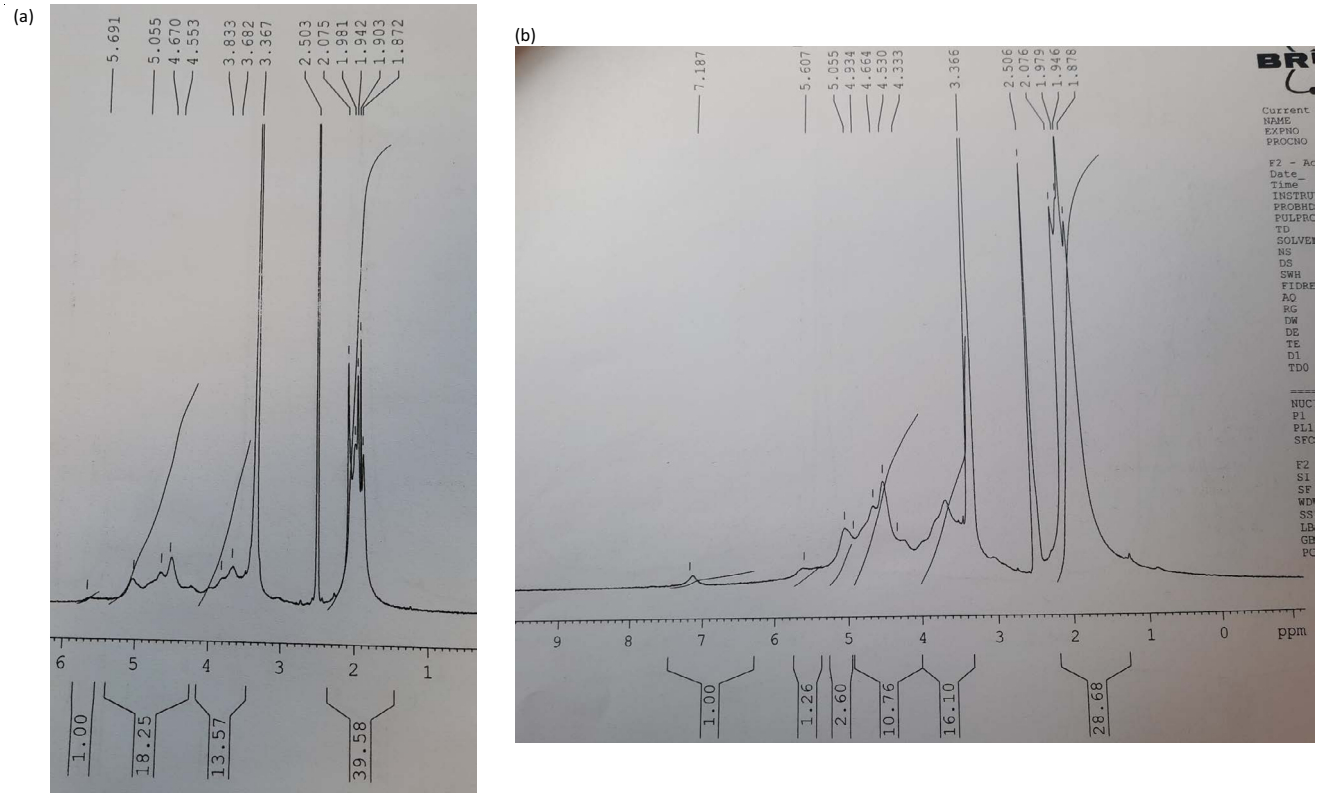

Annexure A: Proton NMR spectra of cellulose acetate based hybrids (a) CA, (b) CA-Al

(c)

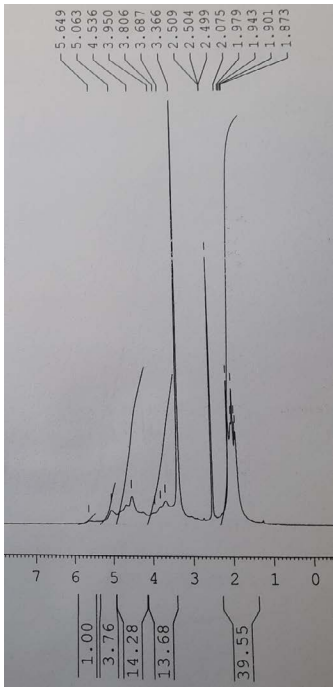

(d)

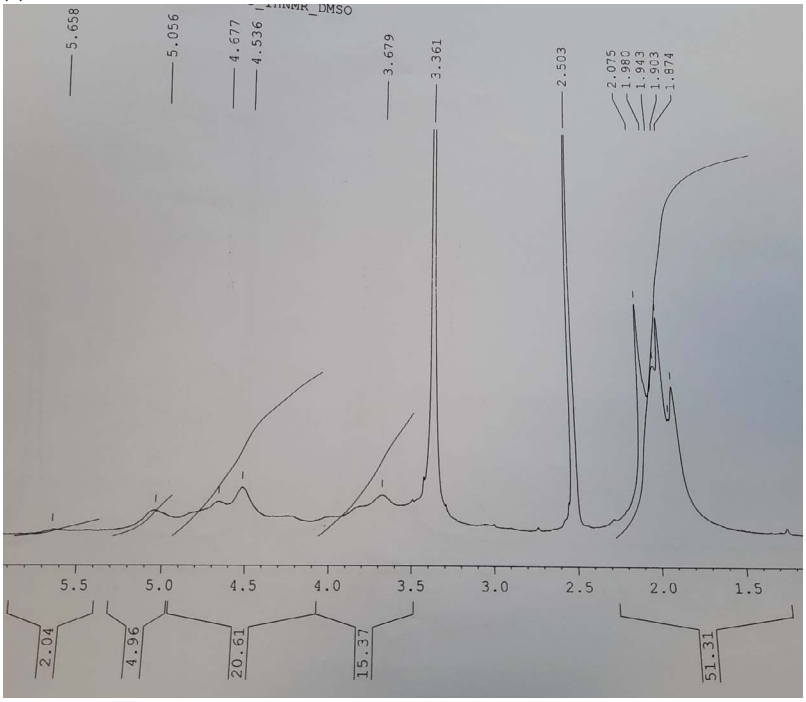

(e)

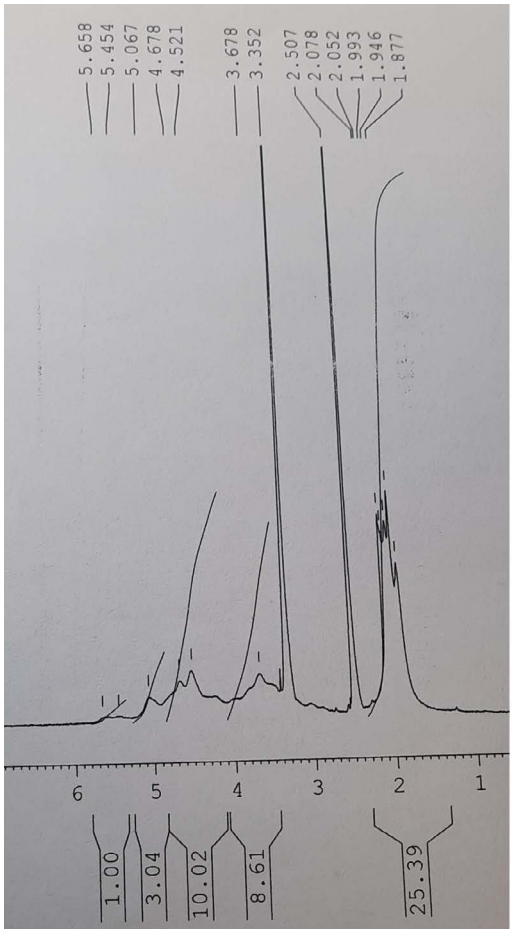

Annexure A: Proton NMR spectra of cellulose acetate based hybrids (c) CA-Si, (d) CA-Ti, and (e) CA-Zr.

(a)

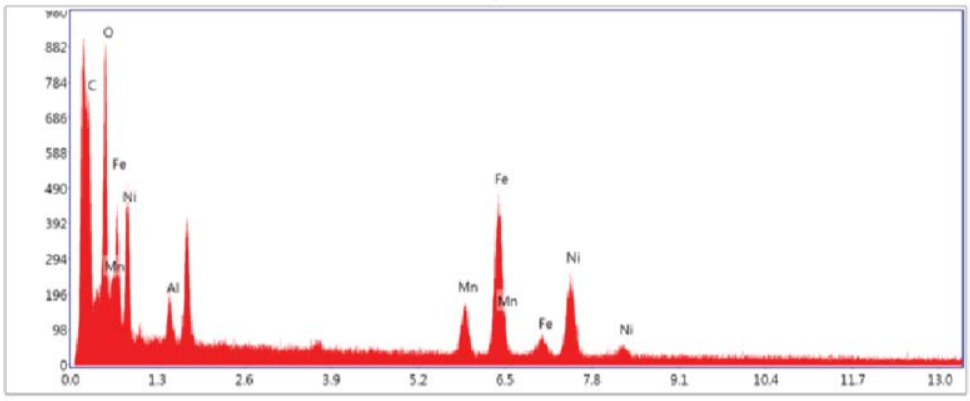

(b)

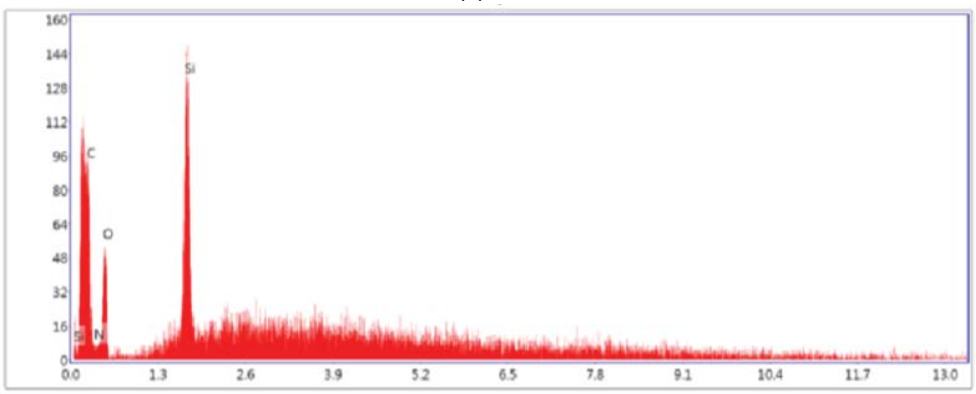

(c)

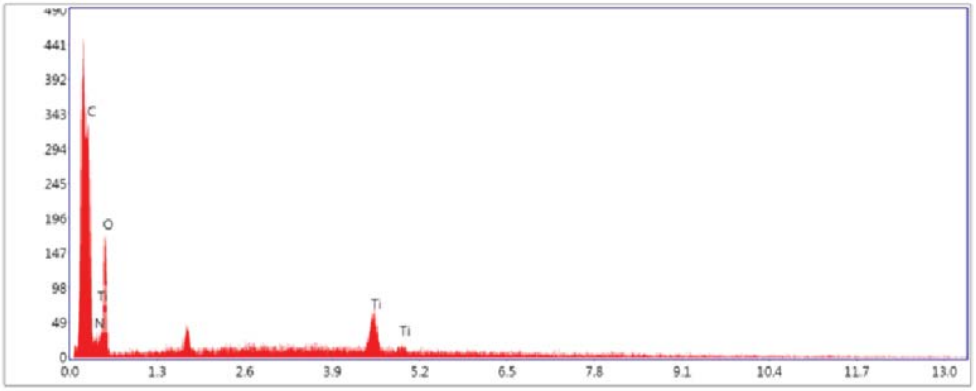

(d)

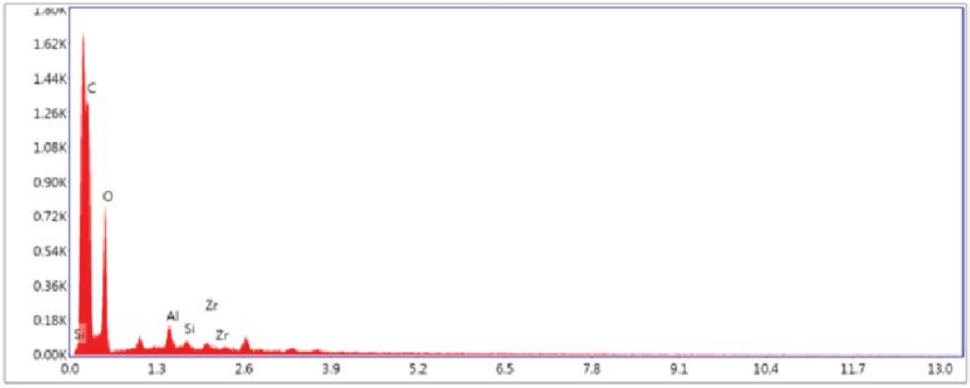

Annexure 2: DES spectrum of cellulose acetate based hybrids (a) CA-Al, (b) CA-Si, (c) CA-Ti, and (d) CA-Zr.